PCCP

Photophysical studies of formic acid in the VUV. Absorption spectrum in the 6–22 eV region†

Sydney Leach,*[a] Martin Schwell,‡[a] Francois Dulieu,[a] Jean-Louis Chotin,[a] Hans-Werner Jochims[b] and Helmut Baumgärtel[b]

[a] *LERMA, Observatoire de Paris-Meudon, 92195, Meudon, France. E-mail: sydney.leach@obspm.fr*

[b] *Institut für Physikalische und Theoretische Chemie der Freien Universität Berlin, Takustr. 3, 14195, Berlin, F.R. Germany*

Received 12th June 2002, Accepted 28th August 2002
First published as an Advance Article on the web 19th September 2002

Absorption spectra of HCOOH were measured between 6 and 22 eV at a maximum resolution of 3 meV. Previous measurements had a spectral limit of 11.7 eV. Analysis and band assignment were aided by data from theoretical calculations on valence and Rydberg states and from photoelectron spectroscopy. Five valence transitions and the different types of Rydberg transitions converging to the ground and the first excited electronic state of $HCOOH^+$ are discussed and assigned in the spectral region below 12.3 eV. Our assignments differ considerably in many aspects from those of previous studies. Observation, analysis and assignment of absorption features between 12 and 22 eV were carried out for the first time. Rydberg bands converging to five expected ionization limits were not observed as discrete features, except for the $3\,^2A'$ ion state, corresponding to promotion of an 8a′ electron. The Rydberg bands converging to the other ionization limits are broad and merge to form broad absorption features. Assignments are made for $n$pa′ ← 8a′ and nda′ ← 8a′ Rydberg transitions, which exhibit discrete absorption bands. It is shown that Rydberg states in the 15.7–16.8 eV region undergo autoionization with a rate $k_{ai} \approx 7.5 \times 10^{13}$ s^{-1} and that this autoionization is probably dissociative.

1. Introduction

Formic acid, HCOOH, is a molecule of concern to both astrophysics and to exobiology. Closely related to possible building blocks of biomolecules,[1] it has been observed by radioastronomy in several sites in the interstellar medium, *e.g.* in the cold dark cloud L134N, as well as (tentative detection) in W51, a region of massive star formation.[2] HCOOH has been proposed as a constituent of icy mantles towards NGC 7538:IRS9,[3] and more recently in the young stellar object W33A at an abundance level of a few percent.[4] Schutte *et al.*[4] indeed suggest that formic acid is a general component of ices occurring in the vicinity of embedded high-mass young stellar objects. Photochemical decomposition products of formic acid, such as the formyl radical HCO, have been observed in interstellar clouds.[5] Although the formic acid ion $HCOOH^+$, or other of the stable isomers of general formula $CH_2O_2^+$ [6,7] have not been observed directly in the interstellar medium, decomposition products such as the formyl radical ion HCO^+, which plays an important role in molecule formation in interstellar clouds,[8] and protonated carbon dioxide, $HOCO^+$, have been observed by radioastronomy.[5] Recently, formic acid has been observed in comets.[9] The relative abundance of formic acid is at least 50 times greater in protostellar ices than in gas phase astronomical sources,[10] including comets, which suggests that the gas phase photostability of formic acid with respect to UV and VUV radiation is much less than for HCOOH embedded in a solid ice. The photophysical properties of HCOOH in the UV and VUV are thus of direct interest for understanding this phenomenon, as well as for undertaking radioastronomy searches, for cometary science and for exobiology studies.

We have carried out a number of photophysical measurements on formic acid, in particular the He I photoelectron spectrum of formic acid and its isotopologues,[11] the ionization quantum yield over the 6–22 eV energy range, the dispersed fluorescence spectrum excited at several VUV photon energies, and excitation spectra for various fluorescence bands.[12] The present work concerns the absorption spectrum of HCOOH between 6 and 22 eV. The absorption results have been important for interpretation of the results of the photophysical investigations. Earlier absorption and fluorescence spectra with comparable resolution were limited to measurements below 11.5 eV.[13,14] Our photoelectron spectra[11] were measured at a higher resolution than in previous studies.[15–17] No previous measurements of the ionization yields of formic acid have been reported. Electron energy loss spectra[18–20] of HCOOH, limited to about 15 eV, did not fully resolve the Rydberg transitions.

2. Experimental

Absorption spectra were measured with an experimental set-up whose essential components and procedure have been described previously[21] so that only a brief resumé is given here. Monochromatised synchrotron radiation was obtained from the Berlin electron storage ring BESSY I (multi-bunch mode) in association with a M-225 McPherson monochromator modified to have a focal length of 1.5 m, and a gold coated laminar Al diffraction grating having 1200 lines mm^{-1}. Spectral dispersion was 5.6 Å mm^{-1}. The monochromator exit slit width was ≈0.1 mm. The 30 cm long absorption cell is separated from the

† Presented at the Second International Meeting on Photodynamics, Havana, Cuba, February 10–16, 2002.

‡ Present address: Laboratoire Interuniversitaire des Systèmes Atmosphériques, Universités Paris 7 et 12, 61 Avenue du Général de Gaulle, 94010 Créteil, France.

monochromator vacuum by a 1 mm thick stainless steel microchannel plate (MCP). Formic acid gas pressures were in the range 20–30 μbar, measured with a Balzers capacitance manometer. No dimer features are expected at the low pressures and the temperature of our formic acid target gas[11,16] and none were observed. The small pressure gradient inside the absorption cell, due to the gas leak through the MCP, does not significantly affect the optical density measurements. The use of the MCP enables us to know the precise optical pathlength, the pressure drop being by a factor of the order of 1000, which ensures linearity in the Beer–Lambert analysis of the optical density measurements. VUV light transmission efficiency of the MCP is estimated to be about 10% and the transmitted light was largely sufficient for absorption measurements. Transmitted radiation strikes a window covered with a layer of sodium salicylate whose ensuing fluorescence was detected by a photomultiplier.

Two scans, one with and one without formic acid gas were carried out for determining the absorption spectrum. During a scan, the VUV light intensity falls off slightly due to continuous loss of electrons in the storage ring. The incident light intensity is furthermore a function of the energy-dependent reflectance of the diffraction grating. These two factors have been taken into account in normalization of the spectra, which were recorded at an energy interval of 6.5 meV.

The optimum energy resolution of our photoabsorption spectra is 3 meV, the precision of the energy scale is ±5 meV. A high resolution VUV photoabsorption spectrum of acetone was used for calibration of the formic acid spectral wavelengths. This acetone spectrum had itself been calibrated with the same monochromator, using mercury emission lines. Commercial HCOOH of highest available purity grade was used without further purification.

3. Results and discussion

3.1. Absorption spectra: General characteristics

The complete absorption spectrum of formic acid between 6 and 22 eV is given in Fig. 1. Features measured in the 7–18 eV region are listed as band numbers, energies and band assignments in Table 1, along with the quantum defects of the Rydberg levels, determined for the origin bands of the Rydberg transitions. The energies of the observed features are quoted to 1 meV and to 1 cm^{-1}; the uncertainties in repeated measurements of the peak frequencies of sharp features are of the order of 10–20 cm^{-1} and those of broad features are somewhat greater. The maximum absorption cross-section of 46.7 Mb occurs in the 17–22 eV region (Fig. 1). Suto *et al.*[13] published absorption spectra over the 4.96–11.7 eV region, and Tabayashi *et al.*[14] in the 8–11.7 eV region, using synchrotron radiation as the spectral source. Our cross-sections for sharp bands are 8–12% higher than those of Suto *et al.*, but are somewhat lower than those of Tabayashi *et al.*, whose measurements have an uncertainty of ±15%. For example, from our measurements the absorption cross sections of the peak of the bands at 8.29 eV (band 3, Table 1) and 10.989 eV (band 70) are 34.6 Mb and 29.8 Mb respectively (ratio 1.16), as compared with 31.9 Mb and 26.6 Mb (ratio 1.20) in Suto *et al.*,[13] 44.1 Mb and 34.4 Mb (ratio 1.28) in Tabayashi *et al.*[14] The differences are not due to different spectral resolutions since visual comparisons of absorption spectra show that our spectral resolution is similar to that of Suto *et al.*[13] and that the absorption spectrum of Tabayashi *et al.*[14] is less well resolved.

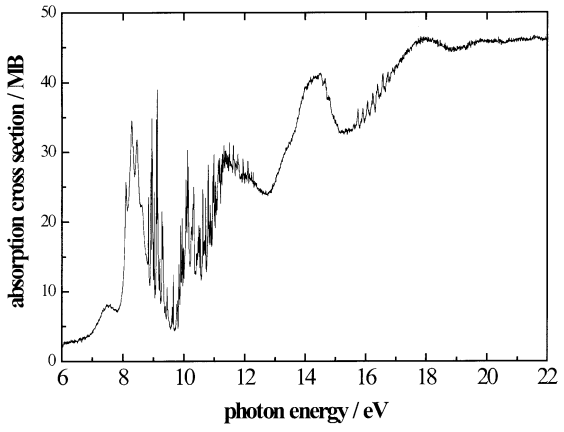

Fig. 1 Overview of the absorption spectrum of HCOOH in the 6–22 eV region.

Bell *et al.*[22] carried out photographic absorption spectroscopy in the 6.9–11.3 eV region and extended previous Rydberg series analyses of Price and Evans.[23] Lower energy absorption spectra below 5.5 eV in the near UV have been studied by Ng and Bell[24] and related photodissociation studies of formic acid have been discussed by Langford *et al.*,[25] who refer also to other low energy absorption studies below 6 eV.

Electron energy loss spectra (EELS) of formic acid have been measured in the 6.5–9.5 eV region[18] and in the 5–16 eV region.[19,20] Conflicting aspects and assignments of valence shell and Rydberg transitions have been discussed on the basis of the respective EELS studies and comparison with optical absorption spectra.[18–20] However, comparison between published EELS spectra and our and other optical absorption spectra clearly indicate that the EELS resolution is insufficient for anything but qualitative discussion.

3.2. Absorption spectra: Theoretical considerations

The distinction between valence and Rydberg transitions is not always easy to establish since there can be quite a lot of mixing between valence and Rydberg states. Our analysis of the absorption spectrum of formic acid seeks to characterise those states that are predominantly valence or predominantly Rydberg in character. For this we use a number of criteria, such as comparison with calculated energies and transition strengths, the nature of the molecular orbitals involved in the optical transitions and their effects on structural and vibrational properties, *etc*. These criteria will be discussed as they arise in this work.

In order to analyse valence and Rydberg transitions in the absorption spectra of formic acid, and to distinguish between them, we first examine the electron configurations and structures of HCOOH and $HCOOH^+$. This aspect is discussed in more detail elsewhere,[11] where it is particularly relevant to analysis of formic acid photoelectron spectra.

3.2.1. HCOOH electron configurations and structures. The ground state of neutral formic acid is planar and belongs to the C_s symmetry group. Its structure, depicted in Fig. 2 from the work of Davis *et al.*,[26] corresponds to the lowest energy isomer, of *cis* (or *anti*) configuration. The *trans* (or *syn*) isomer of HCOOH lies above at 169 meV.[27,28]

The electron configuration of HCOOH is:

$\ldots(6a')^2(7a')^2(8a')^2(1a'')^2(9a')^2(2a'')^2(10a')^2$, $1\,^1A'$

where the bonding characters of the various molecular orbitals are as follows:[11]

$10a'$ is mainly non-bonding n_O on the O atom lone pair of the carbonyl group

$2a''$ is $\pi_{C=O}(\pi_2)$ mixed with n_{OH}, and is mainly localised on the O atom of OH

$9a'$ is σ_{CO} within the O–C–O framework, mixed with n_{OH}, bonding in OH

$1a''$ is $\pi_{CO}(\pi_1)$ mixed with n_{OH}

$8a'$ is σ_{OH}

$7a'$ is σ_{CO}

$6a'$ is σ_{CH}

Table 1 Formic acid absorption features and transition assignments in the 6.8–18 eV spectral region. Quantum defect values are given for the 0_0^0 bands of Rydberg transitions

Band no.	Energy/eV	Frequency ν/cm^{-1}	Assignment	Quantum defect δ
1	7.533	60 757	$\pi^* \leftarrow \sigma_{CO}$ $2\,^1A'' \leftarrow 1\,^1A'$; $3sa' \leftarrow 10a'$	
2	8.106	65 379	$\pi^* \leftarrow \pi_2$ $2\,^1A' \leftarrow 1\,^1A'(0_0^0)$	
3	8.29	66 863	$2\,^1A' \leftarrow 1\,^1A'$ (3_0^1)	
4	8.46	68 234	$2\,^1A' \leftarrow 1\,^1A'$ (3_0^2)	
5	8.622	69 541	$2\,^1A' \leftarrow 1\,^1A'$ (3_0^3)	
6	8.761	70 662	$3sa' \leftarrow 2a''$ (0_0^0)	1.06
7	8.839	71 291	$3pa' \leftarrow 10a'$ (0_0^0)	0.66
8	8.918	71 928	$\pi^* \leftarrow \pi_1$ $3\,^1A' \leftarrow 1\,^1A'(0_0^0)$	
9	8.95	72 186	$\sigma^* \leftarrow n_o$ $4\,^1A' \leftarrow 1\,^1A'(0_0^0)$	
10	8.96	72 267	$3\,^1A' \leftarrow 1\,^1A'$ (9_0^1)	
11	8.983	72 452	$3pa' \leftarrow 10a'$ (5_0^1)	
12	9.026	72 799	$3pa' \leftarrow 10a'$ (3_0^1)	
13	9.059	73 065	$3p'a' \leftarrow 10a'$ (0_0^0)	0.55
14	9.103	73 420	$3\,^1A' \leftarrow 1\,^1A'$ (3_0^1)	
15	9.13	73 638	$4\,^1A' \leftarrow 1\,^1A'$ (3_0^1)	
16	9.147	73 775	$3\,^1A' \leftarrow 1\,^1A'$ $(3_0^1 9_0^1)$	
17	9.165	73 920	$3pa' \leftarrow 10a'$ $(3_0^1 5_0^1)$	
18	9.209	74 275	$3pa' \leftarrow 10a'$ (3_0^2)	
19	9.243	74 549	$3p'a' \leftarrow 10a'$ (3_0^1)	
20	9.28	74 848	$3\,^1A' \leftarrow 1\,^1A'$ (3_0^2)	
21	9.306	75 058	$4\,^1A' \leftarrow 1\,^1A'$ (3_0^2)	
22	9.33	75 251	$3\,^1A' \leftarrow 1\,^1A'$ $(3_0^2 9_0^1)$	
23	9.356	75 461	$3pa' \leftarrow 10a'$ $(3_0^2 5_0^1)$	
24	9.375	75 614	Noise	
25	9.39	75 735	$3pa' \leftarrow 10a'$ (3_0^3)	
26	9.417	75 953	Noise	
27	9.45	76 219	$3\,^1A' \leftarrow 1\,^1A'$ (3_0^3)	
28	9.478	76 445	$4\,^1A' \leftarrow 1\,^1A'$ (3_0^3)	
29	9.50	76 622	$3\,^1A' \leftarrow 1\,^1A'$ $(3_0^3 9_0^1)$	
30	9.598	77 413	?	
31	9.613	77 534	$3\,^1A' \leftarrow 1\,^1A'$ (3_0^4)	
32	9.651	77 840	$3da' \leftarrow 10a'$ (0_0^0)	0.15
33	9.712	78 332	Noise	
34	9.744	78 590	Noise	
35	9.763	78 744	$3pa' \leftarrow 2a''$ (0_0^0)	0.72
36	9.782	78 897	$3\,^1A' \leftarrow 1\,^1A'$ (3_0^5)	
37	9.826	79 252	Noise	
38	9.835	79 324	$3da' \leftarrow 10a'$ (3_0^1)	
39	9.854	79 477	?	
40	9.891	79 776	$3pa' \leftarrow 2a''$ (6_0^1)	
41	9.942	80 187	$3pa'' \leftarrow 2a''$ (0_0^0)	0.64
42	9.987	80 550	$4sa' \leftarrow 10a'$ (0_0^0)	0.81
43	10.016	80 784	$3da' \leftarrow 10a'$ (3_0^2)	
44	10.053	81 083	$3pa' \leftarrow 2a''$ (3_0^2)	
45	10.071	81 228	$3pa'' \leftarrow 2a''$ (6_0^1)	
46	10.086	81 349	$3pa'' \leftarrow 2a''$ (5_0^1)	
47	10.125	81 663	$4sa' \leftarrow 10a'$ (6_0^1)	
48	10.147	81 841	$4pa' \leftarrow 10a'$ (0_0^0)	0.60
49	10.17	82 026	$4sa' \leftarrow 10a'$ (3_0^1)	
50	10.256	82 720	Broad overlapping features $3pa'' \leftarrow 2a''$ (3_0^1)	
51	10.299	83 067	$4pa' \leftarrow 10a'$ (6_0^1)	
52	10.324	83 268	$4pa' \leftarrow 10a'$ (3_0^1)	
53	10.375	83 680	$4p'a' \leftarrow 10a'$ (0_0^0)	0.22
54	10.41	83 962	$4da' \leftarrow 10a'$ (0_0^0)	0.14
55	10.422	84 220	$4pa' \leftarrow 10a'$ (6_0^2)	
56	10.47	84 446	$4pa' \leftarrow 10a'$ $(3_0^1 6_0^1)$	
57	10.498	84 672	$4pa' \leftarrow 10a'$ (3_0^2)	
58	10.533	84 954	$5sa' \leftarrow 10a'$ (0_0^0)	0.85
59	10.595	85 454	$4da' \leftarrow 10a'$ (3_0^1)	
60	10.621	85 664	$5pa' \leftarrow 10a'$ (0_0^0)	0.60
61	10.653	85 922	$4pa' \leftarrow 10a'$ $(3_0^2 6_0^1)$	
62	10.684	86 172	$5sa' \leftarrow 10a'$ (6_0^1)	
63	10.717	86 438	$5sa' \leftarrow 10a'$ (3_0^1); $3da'' \leftarrow 2a''$ (0_0^0)	0.14
64	10.769	86 857	$5da' \leftarrow 10a'$ (0_0^0)	0.05
65	10.78	86 946	$4da' \leftarrow 10a'$ (3_0^2)	
66	10.806	87 156	$6sa' \leftarrow 10a'$ (0_0^0); $5pa' \leftarrow 10a'$ (3_0^1)	0.88
67	10.86	87 591	$6pa' \leftarrow 10a'$ (0_0^0); $4sa' \leftarrow 2a''$ (0_0^0)	0.59; 1.01
68	10.898	87 898	$5sa' \leftarrow 10a'$ (3_0^2)	

Table 1 (continued)

Band no.	Energy/eV	Frequency ν/cm^{-1}	Assignment	Quantum defect δ
69	10.956	88 366	$7sa' \leftarrow 10a'$ (0_0^0); $5da' \leftarrow 10a'$ (3_0^1); $5pa' \leftarrow 10a'$ $(3_0^1 6_0^1)$	0.93
70	10.989	88 632	$6sa' \leftarrow 10a'$ (3_0^1); $7pa' \leftarrow 10a'$ (0_0^0); $4sa' \leftarrow 2a''$ (6_0^1)	0.63
71	11.014	88 833	$3da'' \leftarrow 2a''$ (3_0^1)	
72	11.045	89 083	$8sa' \leftarrow 10a'$ (0_0^0); $6pa' \leftarrow 10a'$ (3_0^1)	1.03
73	11.077	89 342	$8pa' \leftarrow 10a'$ (0_0^0)	0.59
74	11.123	89 713	Noise	
75	11.134	89 801	$7sa' \leftarrow 10a'$ (3_0^1); $9pa' \leftarrow 10a'$ (0_0^0)	0.55
76	11.148	89 914	$4pa'' \leftarrow 2a''$ (0_0^0); $4sa' \leftarrow 2a''$ (3_0^1)	0.67
77	11.178	90 156	$6sa' \leftarrow 10a'$ (3_0^2); $7pa' \leftarrow 10a'$ (3_0^1)	
78	11.193	90 277	$8sa' \leftarrow 10a'$ (6_0^1)	
79	11.233	90 600	$8sa' \leftarrow 10a'$ (3_0^1); $6pa' \leftarrow 10a'$ (3_0^2)	
80	11.264	90 850	$8pa' \leftarrow 10a'$ (3_0^1)	
81	11.298	91 124	?	
82	11.317	91 277	$9pa' \leftarrow 10a'$ (3_0^1)	
83	11.34	91 463	?	
84	11.356	91 592	?	
85	11.378	91 769	?	
86	11.402	91 963	?	
87	11.417	92 084	?	
88	11.444	92 302	$8pa' \leftarrow 10a'$ (3_0^2); $4da'' \leftarrow 2a''$ (0_0^0)	0.18
89	11.489	92 665	?	
90	11.497	92 729	$5sa' \leftarrow 2a''$ (0_0^0)	1.07
91	11.531	93 003	$3pa' \leftarrow 9a'$ (0_0^0)	0.72
92	11.628	93 786	$5sa' \leftarrow 2a''$ (6_0^1)	
93	11.65	93 963	$5pa'' \leftarrow 2a''$ (0_0^0)	0.68
94	11.712	94 463	$4da'' \leftarrow 2a''$ (3_0^1); $3pa' \leftarrow 9a'$ (3_0^1)	
95	11.781	95 020	$5pa'' \leftarrow 2a''$ (6_0^1); $5sa' \leftarrow 2a''$ (3_0^1)	
96	11.795	95 133	$5da'' \leftarrow 2a''$ (0_0^0)	0.17
97	11.809	95 245	?	
98	11.83	95 415	$6sa' \leftarrow 2a''$ (0_0^0)	1.02
99	11.893	95 923	$6pa'' \leftarrow 2a''$ (0_0^0); $3pa' \leftarrow 9a'$ (3_0^2)	0.70
100	11.946	96 350	$5pa'' \leftarrow 2a''$ (3_0^1)	
101	11.958	96 447	$6sa' \leftarrow 2a''$ (6_0^1)	
102	11.988	96 689	$7sa' \leftarrow 2a''$ (0_0^0)	1.09
103	12.026	96 996	$7pa'' \leftarrow 2a''$ (0_0^0); $6pa'' \leftarrow 2a''$ (6_0^1)	0.78
104	12.058	97 254	$5pa'' \leftarrow 2a''$ $(3_0^1 6_0^1)$; $5sa' \leftarrow 2a''$ (3_0^2)	
105	12.094	97 544	$8sa' \leftarrow 2a''$ (0_0^0)	1.07
106	12.116	97 722	$7sa' \leftarrow 2a''$ (6_0^1); $6sa' \leftarrow 2a''$ (3_0^1)	
107	12.159	98 068	$7pa'' \leftarrow 2a''$ (6_0^1)	
108	12.221	98 568	$8sa' \leftarrow 2a''$ (6_0^1)	
109	12.286	99 093	$7sa' \leftarrow 2a''$ (3_0^1) ?	
110	13.48	108 722	$? \leftarrow 9a'$[a]	
111	14.49	116 869	$3pa' \leftarrow 8a'$ (0_0^0)	0.67
112	14.65	118 160	? (broad feature)	
113	14.785	119 248	? (broad feature)	
114	15.746	126 999	$4pa' \leftarrow 8a'$ (0_0^0)	0.67
115	15.908	128 306	$4pa' \leftarrow 8a'$ (6_0^1)	
116	16.064	129 564	$4da' \leftarrow 8a'$ (0_0^0)	0.125
117	16.238	130 968	$5pa' \leftarrow 8a'$ (0_0^0)	0.69
118	16.399	132 266	$5pa' \leftarrow 8a'$ (6_0^1); $5da' \leftarrow 8a'$ (0_0^0)	0.124
119	16.48	132 919	$6pa' \leftarrow 8a'$ (0_0^0)	0.74
120	16.57	133 645	$6da' \leftarrow 8a'$ (0_0^0)	0.176
121	16.624	130 081	$7pa' \leftarrow 8a'$ (0_0^0)	0.74
122	16.682	134 549	$7da' \leftarrow 8a'$ (0_0^0)	0.14
123	16.734	134 968	$8pa' \leftarrow 8a'$ (0_0^0)	See text
124	17.90[b]	144 372	$? \leftarrow 6a'$[b]	

[a] Region of broad overlapping Rydberg bands converging to the 2 ^{2}A′ ion state. [b] Maximum of broad overlapping Rydberg bands converging to the 5 ^{2}A′ ion state.

The two lowest unoccupied molecular orbitals, whose calculated relative energies depend strongly on the basis set used[11b] are:

3a″, which is a π* molecular orbital

11a′ which is the antibonding in OH analogue of orbital 9a′.

The 1 ^{2}A′ ground state of the ion, whose ionization energy (IE) is 11.3246 eV,[11] has the electron configuration: …$(6a')^2(7a')^2(8a')^2(1a'')^2(9a')^2(2a'')^2(10a')$, and is planar.[7,22,29,30] The 1 ^{2}A″ first excited electronic state of the ion, at 12.378 eV,[11] of configuration …$(6a')^2(7a')^2(8a')^2(1a'')^2(9a')^2(2a'')(10a')^2$, is also planar.[7,11,29,30] The characteristics of higher excited states of the formic acid ion will be discussed later, in section 4.

Table 2 gives the vibrational modes and frequencies of neutral formic acid in its ground state, based on the IR and Raman spectra of several groups,[11,31–33] and the corresponding values determined for the cation ground state 1 ^{2}A′ and

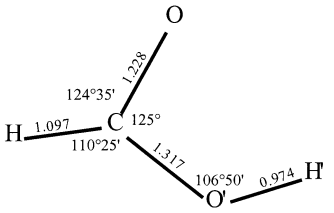

Fig. 2 Structure of the ground state of HCOOH. Internuclear distances in Å.

first excited state $1\,^2A''$ by analysis of the He I photoelectron spectra of formic acid.[11b] Vibrational frequencies of higher excited ion states, determined from photoelectron spectra, will be discussed in section 4.

3.2.2. Valence states and transitions of HCOOH. We will be concerned with the five valence transitions discussed below:

(1) The lowest energy singlet–singlet valence transition, $\ldots(9a')^2(2a'')^2(10a')^2$, $1\,^1A' \rightarrow \ldots(9a')^2(2a'')^2(10a')(3a'')$, $1\,^1A''$ corresponds to a $\pi^* \leftarrow n_O$ transition and is calculated to have an energy between 5 and 7 eV (Table 3). It is also predicted to be a weak transition whose oscillator strength is calculated by Basch *et al.*[37] to be $f \approx 0.007$, and by Demoulin[35] to be $f = 0.014$, *i.e.* 2.9% of his calculated oscillator strength, $f = 0.494$ (the value given by Demoulin, 0.0494, is an obvious misprint), of the strongest valence transition, $\pi^* \leftarrow \pi_{C=O}(\pi_2)$ (see below). Demoulin's dipole length calculations are not expected to give accurate values of the oscillator strengths, because of insufficient configuration interaction, but the relative values are probably of qualitative significance. The experimental oscillator strength of the $\pi^* \leftarrow \pi_{C=O}(\pi_2)$ transition is $f \approx 0.2$ (see section 3.3.2) so that, based on the relative intensities calculated by Demoulin, the oscillator strength of the $1\,^1A'' \leftarrow 1\,^1A'$ transition would be of the order of $f = 0.006$, and this is indeed close to the theoretical estimation of Basch *et al.* We remark also that the upper state is of A'' symmetry so that the electronic transition is polarized perpendicular to the molecular plane and is thus expected to be of relatively low intensity.[38]

Although the lowest energy singlet–singlet valence transition is outside our spectral observation range, its properties can be used as an initial test of our methodological approach. From the nature of the HOMO (10a') and LUMO (3a''), in this first valence transition one expects a lengthening of the C=O bond and a decrease in the C=O stretching frequency ν_3 whose ground state value is 1777 cm^{-1} [32] (Table 2). Experimentally, the electronic origin of this transition is at 4.64 eV [39] and it is reported, from EELs measurements,[19] to be a weak transition having an intensity about 1% that of the $\pi^* \leftarrow \pi_{C=O}(\pi_2)$ transition, in agreement with our relative intensities discussion above. Spectroscopic analysis shows that the C=O bond length increases from 1.288 Å in the ground state to 1.407 Å in the $1\,^1A''$ state[24] and the ν_3 C=O stretching frequency decreases from 1777 cm^{-1} to 1115 cm^{-1},[39] in agreement with our predictions.

There are some other marked changes, in particular in bond angles and in vibrational frequencies, following the $1\,^1A'' \leftarrow 1\,^1A'$ absorption transition. The OCO' bond angle decreases from 125° to 111.4°,[25] the OCO' bending frequency goes from $\nu_7'' = 625$ cm^{-1} to $\nu_7' = 404$ cm^{-1},[39] the formyl hydrogen becomes non-planar (out-of-plane angle is 32°, with both H atoms twisted out of the plane defined by the O–C=O backbone in an *anti*-configuration[25]) and the corresponding out-of-plane OH' vibration drops from $\nu_9'' = 642$ cm^{-1} to $\nu_9' = 251$ cm^{-1}.[39] These changes are in line with expectations from the respective bonding characteristics of the HOMO and LUMO orbitals. Since the HOMO is mainly a carbonyl oxygen σ lone pair, we can deduce that the tendency to non-planarity is associated with the 3a'' LUMO. This is consistent with the fact that the ground and the first excited state of the $HCOOH^+$ ion, which correspond respectively to removal of an electron from the 10a' and 2a'' molecular orbitals, are both planar.[7,11] Other valence excitations to the 3a'' orbital might therefore induce non-planarity in the corresponding excited state.

HCOOH is pyramidal in shape in the $1\,^1A''$ excited state.[24] If inversion can occur easily in this electronic state, the relevant permutation group becomes isomorphous with C_s, so that the C_s symmetry labelling still applies, in particular the distinction between a' and a'' symmetries is conserved. Thus the observation[39] that the 9_0^1 band in the $1\,^1A'' \leftarrow 1\,^1A'$ transition is three times more intense than the 0_0^0 band can be understood in that, since ν_9' has a'' symmetry, the total symmetry of the upper state vibronic level of the 9_0^1 band will be a', *i.e.* polarized in the pseudo-plane of the molecule, and thus intensity enhanced.

From the good correspondence between the experimental and our predicted structural changes in the first valence transition, we conclude that the approach we have taken is valid concerning the relation between HCOOH structural changes and the molecular orbitals involved in the electronic transition, at least for the valence transitions of formic acid.

(2) The second valence transition, $2\,^1A' \leftarrow 1\,^1A'$, corresponds to the $\pi^* \leftarrow \pi_{C=O}(\pi_2)$ transition (Table 3), and is predicated by most calculations to be a strong transition in the 9–10 eV region. As mentioned earlier, its experimental oscillator strength is $f \approx 0.2$. The value calculated by Basch *et al.*[37] is $f = 0.214$ or 0.755 according to whether the dipole velocity operator or the dipole length operator is used. The large difference between these two values indicates that the wave functions used for the state energy calculations are not optimal. In fact, Basch *et al.* calculate an energy of 12.02 eV for this transition, much higher than other calculated values (Table 3). We note that the $2\,^1A'$ state is considered to have a substantial contribution of the $\ldots(9a')^2(2a'')^2(10a')(11a')$ configuration.[36]

Table 2 Experimental vibrational modes and frequencies of the $1\,^1A'$ ground state of HCOOH,[a] and the $1\,^2A'$ ground state and first excited $1\,^2A''$ state of $HCOOH^+$ [b]

Symmetry	Mode number	Mode type	HCOOH $1\,^1A'$ ν/cm^{-1}	$HCOOH^+$ $1\,^2A'$ ν/cm^{-1}	$HCOOH^+$ $1\,^2A''$ ν/cm^{-1}
a'	ν_1	ν(OH)	3569		
a'	ν_2	ν(CH)	2942	3026	3232
a'	ν_3	ν(CO)	1777	1495	2343
a'	ν_4	δ(HCO)	1381		1398
a'	ν_5	δ(H'O'C)	1223	1196	1324
a'	ν_6	ν(CO)	1104	1196	1029
a'	ν_7	δ(OCO')	625	510	574
a''	ν_8	δ(CH)	1033		
a''	ν_9	δ(OH)	642		

[a] From IR and Raman data.[11,31–33] [b] From He I photoelectron spectra.[11b]

Table 3 Valence transitions in formic acid: calculated and experimental transition energies

Transitions between electronic states	Transitions between molecular orbitals	Orbital character	Calculated transition energy/eV	Experimental transition energy/eV
$1\,^1A'' \leftarrow 1\,^1A'$	$3a'' \leftarrow 10a'$	$\pi^* \leftarrow n_o$	5.24[35] 5.8[34] 5.83[36] 6.0[19] 6.86[37]	4.64[39]
$2\,^1A' \leftarrow 1\,^1A'$	$3a'' \leftarrow 2a''$	$\pi^* \leftarrow \pi_{C=O}$	8.9[19] 9.52[34] 9.64[35] 9.84[36] 12.02[37]	8.107 [present study]
$2\,^1A'' \leftarrow 1\,^1A'$	$3a'' \leftarrow 9a'$	$\pi^* \leftarrow \sigma_{CO}$	8.9[19] 9.39[35] 10.43[34] 11.2[37]	≈7.53 (max) [present study, see text]
$3\,^1A' \leftarrow 1\,^1A'$	$3a'' \leftarrow 1a''$	$\pi^* \leftarrow \pi_{C-O}$	11.6[19] 12.72[35] 13.6[34] 14.95[37]	8.919 [present study]
$4\,^1A' \leftarrow 1\,^1A'$	$11a' \leftarrow 10a'$	$\sigma^* \leftarrow n_O$	12.84[37] 15.18[34]	8.95 [present study]

From the nature of the HOMO-1 (2a″) and the LUMO (3a″) one would expect on excitation a lengthening of the C=O bond and a decrease in the C=O stretching frequency ν_3, a lengthening of the OH bond and decrease in its stretching frequency ν_1 ($=3569$ cm^{-1} in the ground state), and a possible non-planarity of the upper state. We discuss later our reasons for assigning bands in the 8–8.8 eV region as the $\pi^* \leftarrow \pi_{C=O}(\pi_2)$ transition (Tables 1 and 3) and the nature of the structural changes induced in the excited state.

(3) The third valence transition, $2\,^1A'' \leftarrow 1\,^1A'$, is the $\pi^* \leftarrow \sigma_{CO}$ transition, whose energy is calculated to be fairly close to the $\pi^* \leftarrow \pi_{C=O}(\pi_2)$ transition (Table 3). It is also predicted to be a weak transition polarized perpendicular to the molecular plane. From the nature of the HOMO-2 (9a′) and the LUMO (3a″) one would expect on excitation a lengthening of the C–O bond and a decrease in the C–O stretching frequency ν_6, a lengthening of the OH bond and decrease in its stretching frequency ν_1 ($=3569$ cm^{-1} in the ground state), and a possible non-planarity of the upper state.

Experimentally, as discussed later, we consider that this transition is either too weak to be observed or that it occurs within, and is dominated by, the broad absorption band at about 7.5 eV, which is essentially due to the $3sa' \leftarrow 10a'$ Rydberg transition. If this valence transition does occur in the 7.5 eV region, it implies that, on a single configuration basis, the energy order of the 9a′ and 2a″ molecular orbitals are reversed with respect to the electronic configuration of the ground state given previously. We note that the calculations of Demoulin[35] also place the $2\,^1A'' \leftarrow 1\,^1A'$ absorption transition at a lower energy than $2\,^1A' \leftarrow 1\,^1A'$. Furthermore, this order is also predicted for the analogous transitions in several other HCOX species.[37]

(4) The fourth valence transition, $3\,^1A' \leftarrow 1\,^1A'$, corresponds to the $\pi^* \leftarrow \pi_{CO}(\pi_1)$ transition (Table 3). It is calculated to have an energy at least 2 eV above that of the $\pi^* \leftarrow \pi_{C=O}(\pi_2)$ transition. Basch *et al.*[37] calculate $f = 0.070$ (dipole velocity operator), $f = 0.209$ (dipole length operator). The oscillator strength of this transition is predicted to be between 10% and 40% as intense as the $\pi^* \leftarrow \pi_2$ transition.[19,35]

From the nature of the HOMO-3 (1a″) and the LUMO (3a″) one would expect on excitation a lengthening of the carbon–oxygen bonds and a decrease in their stretching frequencies, as well as a possible non-planarity of the upper state. Experimental assignments of this transition are discussed later.

(5) The fifth valence transition, $4\,^1A' \leftarrow 1\,^1A'$, corresponds to a $\sigma^* \leftarrow n_O$ transition (Table 3), predicted to be at higher energy than $\pi^* \leftarrow \pi_{CO}(\pi_1)$, and to be a fairly strong transition, of calculated oscillator strength $f = 0.113$ (dipole velocity operator), $f = 0.214$ (dipole length operator).[37]

The 11a′ LUMO+1 orbital is OH antibonding so that we expect a lengthening of the O–H bond and a decrease in the OH stretch frequency ν_1. Following the previous discussion concerning the $2\,^1A'$ state, the $4\,^1A'$ excited state arising from the $11a' \leftarrow 10a'$ orbital excitation presumably has a contribution from the $(9a')^2(2a'')\,(10a')^2(3a'')$ configuration. This would lead to a tendency to lengthen the C=O bond with a consequent decrease in the C=O stretching frequency ν_3, but probably not as much as in the $2\,^1A'$ state, and to a possible non-planarity of the upper state $4\,^1A'$. The possible experimental assignments of this $4\,^1A \leftarrow 1\,^1A'$ valence transition are considered later.

The excited states discussed so far are nominally valence states, the spatial extent of their upper molecular orbitals, as measured by $\langle r^2\rangle^{1/2}$,[35] being expected to be of the order of 3 a_0. However the dimensions of some of the HCOOH valence states can be closer to those of Rydberg states, *e.g.* the $2\,^1A'$ and $3\,^1A'$ states are calculated to have $\langle r^2\rangle^{1/2}$ values of 6.6 and 8.7 a_0 respectively,[35] which are of the order of the calculated size of some of the $n = 3$ Rydberg states of formic acid. This may indicate the existence of some valence–Rydberg mixing for these two states.

3.2.3. Rydberg states and transitions of HCOOH. We will initially be concerned with two main classes of Rydberg transitions in formic acid, those involving promotion of a 10a′ orbital electron leading at $n = \infty$ to the ion ground state $1\,^2A'$, and those where promotion of a 2a″ orbital electron leads eventually to the first excited state $1\,^2A''$ of the ion. Rydberg transitions involving higher energy ionization limits are discussed in section 4.

There are various possible Rydberg series corresponding to transitions to nondegenerate s orbitals and to split core p and d orbitals. The Rydberg series transitions leading to the ground state of the ion are:

$n$sa′ ← 10a′;

$n$pa′ ← 10a′; $n$pa″ ← 10a′; $n$pa′ ← 10a′

$n$da′ ← 10a′; $n$da″ ← 10a′; $n$da′ ← 10a′; $n$da″ ← 10a′, $n$da′ ← 10a′,

the transitions being $^1A' \leftarrow 1\,^1A'$ when the Rydberg orbital has a′ symmetry, and $^1A'' \leftarrow 1\,^1A'$ when it has a″ symmetry.

Rydberg transitions that can lead to the first excited state are:

$n$sa′ ← 2a″;

$n$pa′ ← 2a″; $n$pa″ ← 2a″; $n$pa′ ← 2a″

$n$da′ ← 2a″; $n$da″ ← 2a″; $n$da′ ← 2a″; $n$da″ ← 2a″; $n$da′ ← 2a″,

the transitions here being $^1A' \leftarrow 1\,^1A'$ when the Rydberg orbital has a″ symmetry, and $^1A'' \leftarrow 1\,^1A'$ when it has a′ symmetry.

The maximum oscillator strength for a Rydberg transition is found empirically to be $f = 0.08$ per spatial degeneracy.[38] Furthermore, f should vary with n^{-3}, a relation that we can use as a guide in Rydberg assignments. Another useful criterion is that transitions to $^1A''$ states should be much weaker than to $^1A'$ states.

The Rydberg series absorption bands should have upper states whose geometry is similar to that of the formic acid ion state to which they converge at their limits. The electron configuration of the $1\,^2A'$ ground state of the ion leads us to conjecture that in the Rydberg series leading to this ion state, we should find progressions in ν_3 with frequency diminished with respect to ν_3(C=O) = 1777 cm^{-1} in the neutral ground state, as well as progressions in ν_6(C–O) with frequency increased with respect to the neutral ground state ν_6(C–O) = 1104 cm^{-1}. This is indeed what is found in the He I photoelectron spectrum of HCOOH,[11] where we also see excitation of $\nu_7'(\delta(\mathrm{OCO}))$.

In the $1\,^2A''$ excited state of the ion, removal of the 2a″ electron from the neutral ground state configuration should lead to an increase in the C=O bond length, a decrease in the C–O bond length and marked increases in the H′O′C and HCO′ angles, as well as a decrease in the OCO′ angle. We therefore expect to see a decrease in one of the two carbon–oxygen stretch vibrations and an increase in the other, besides excitation of ν_7. The actual behaviour of the carbon–oxygen stretch vibrations in the He I PES of formic acid and its isotopomers[11b] is more complex than these expectations, in particular because of structural flexibility in this excited state that is not taken into account in considering only the properties of the molecular orbitals in this species. The appropriate frequencies to look for in vibronic bands of Rydberg series converging to this state of the $HCOOH^+$ ion are those given for the $1\,^2A''$ state modes in Table 2.

3.3. Spectral assignments: Valence and Rydberg transitions below the ion ground state

Successive sections of the absorption spectra between 6.8 and 17.5 eV are shown in Figs. 3–7. The band assignments are listed in Table 1 but, for the sake of visual clarity, not all assignments are indicated in the figures. The various spectral regions are discussed in turn, beginning with the valence and Rydberg transitions below the ion ground state energy.

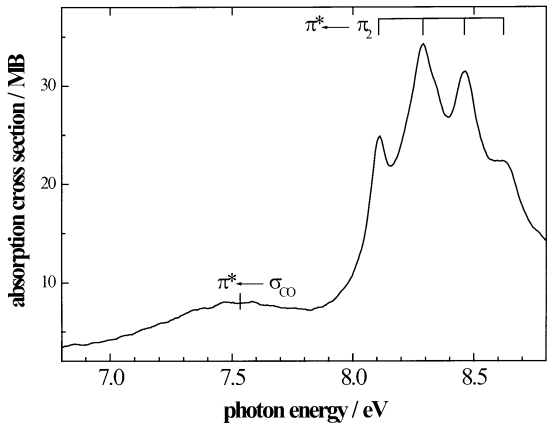

Fig. 3 HCOOH absorption spectrum: 6.8–8.8 eV.

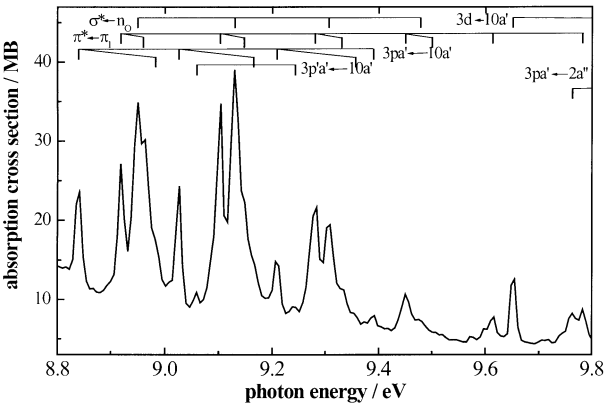

Fig. 4 HCOOH absorption spectrum: 8.8–9.8 eV.

3.3.1. The 7.5 eV band. Fig. 3 shows the absorption spectrum of formic acid between 6.8 and 8.7 eV. The continuum with a maximum around 7.5 eV, known in the literature as the Ã′ band,[22] has been assigned by Fridh[19] and by Ari and Güven[20] as the 3sa′ ← 10a′ Rydberg transition. Barnes and Simpson[40] on the basis of band filiation in related compounds containing the carbonyl or carboxyl group, have assigned the Ã′ band to the $\pi^* \leftarrow n'_O$ transition ($= \pi^* \leftarrow \sigma_{CO}$, see below) where n′ is the second lone pair orbital on the carbonyl group oxygen. Since n′ is something like a 2p orbital extending along the C–O line,[41,42] the n'_o orbital can be considered as equivalent to the σ(CO) orbital discussed above. On the other hand, Nagakura *et al.*[43] have assigned this band to the $\pi^* \leftarrow \pi_2$ transition. However, as discussed below, our analysis concludes that the $\pi^* \leftarrow \pi_2$ transition lies in the 8–8.8 eV region.

The $\pi^* \leftarrow \sigma_{CO}$ transition $2\,^1A'' \leftarrow 1\,^1A'$ (Table 3) is predicted to be considerably less intense than the $\pi^* \leftarrow \pi_2$ transition.[37] As discussed earlier, it may be too weak to be observed or it may lie within the broad 7.5 eV feature which we consider to mainly correspond to a diffuse 3sa′ ← 10a′ Rydberg transition. This is supported by the experimental oscillator strength of the 7.5 eV band, determined by the formula $f \approx 9.7 \times 10^{-3} \times \sigma_{max} \times \Delta E_{1/2}$, where the peak absorption cross section is in Mb, and $\Delta E_{1/2}$ is the FWHM, in eV, of an assumed Gaussian band profile. The value thus obtained, $f \approx 0.025$, is six times greater than $f = 0.004$ calculated for the $2\,^1A'' \leftarrow 1\,^1A'$ transition,[37] and is thus consistent with the existence,

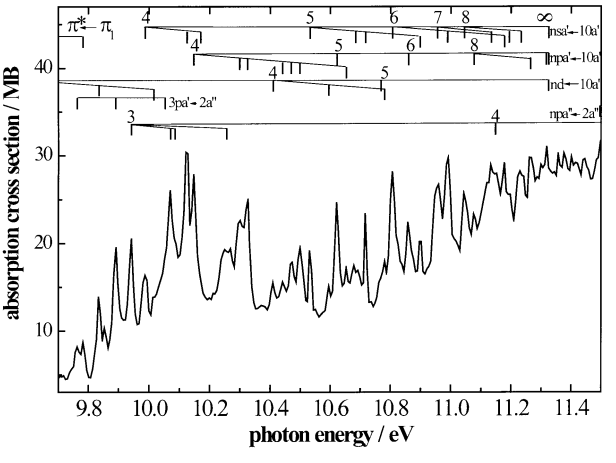

Fig. 5 HCOOH absorption spectrum: 9.7–11.5 eV.

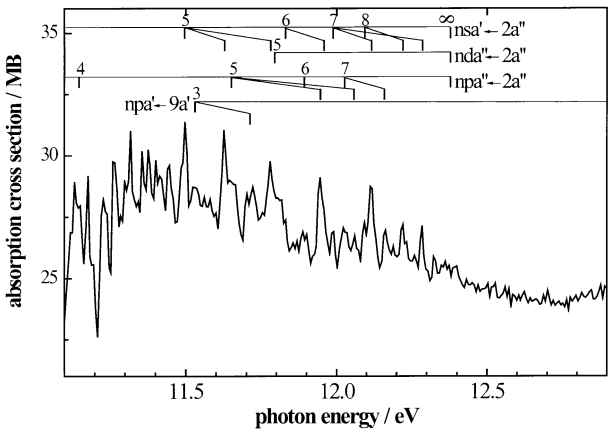

Fig. 6 HCOOH absorption spectrum: 11.1–12.9 eV.

within the 7.5 eV band, of both this valence transition and the 3sa′ ← 10a′ Rydberg transition.

Insofar as the $2\,^1A'' \leftarrow 1\,^1A'$ transition occurs within the 7.5 eV band, the broadness of this band may be associated in part with promotion of an electron from the 9a′ to the 3a″ orbital, since in the He I photoelectron spectrum of formic acid, ionization by removal of an electron from the 9a′ orbital gives rise to a broad mainly featureless PES band at about 14.6 eV, although the next two higher energy PES bands, involving ionization of other electrons, show vibrational structure.[11b,15]

3.3.2. The 8.0–8.8 eV region bands. The structured absorption in the 8–8.8 eV region (Fig. 3), has four component bands, at 8.106, 8.290, 8.460 and 8.622 eV. Although much less broad than the feature at 7.5 eV, these bands are nevertheless broader than the sharp features in the 9 eV region. There have been various interpretations of these bands. They have been assigned[13,22] as vibrational components of the 3s ← 10a′ Rydberg transition ($n = 3$ of an ns series whose quantum defect is $\delta = 0.85$). The argument of Bell *et al.*[22] in favour of this Rydberg assignment is that the absorption bands in the 8.4 eV region ressemble the first photoelectron spectrum band of formic acid, as measured by Brundle *et al.*[15] This is certainly true, even though the band intervals in the respective spectra indicate that the resemblance may be more qualitative than quantitative (see below). However, an examination of Fig. 2 of Brundle *et al.*,[15] which gives a direct comparison of absorption and photoelectron bands, shows that the absorption band being compared in their work is *not* the 8.4 eV band system but the sharp band system beginning at 8.84 eV (see below). A further argument against the Bell *et al.* assignment is that it leads to an unreasonably small term value for the 3s level.[38]

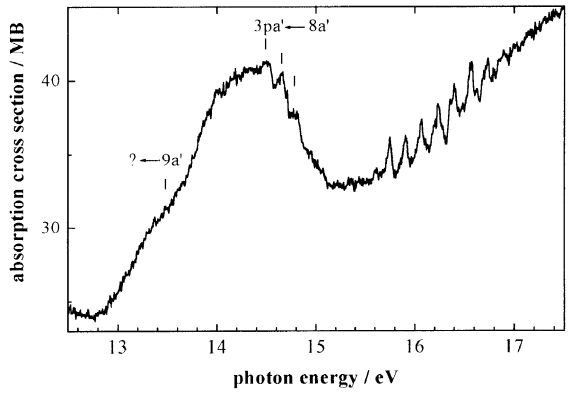

Fig. 7 HCOOH absorption spectrum: 12.5–17.5 eV.

Several authors[14,20,40] assign the bands in the 8–8.8 eV region to the $\pi^* \leftarrow \pi_2$ transition, *i.e.* $2\,^1A' \leftarrow 1\,^1A'$, whereas Fridh[19] considers the transition to be part of the $n$pa′σ Rydberg series (see below). The successive member intervals of the four bands are 1484, 1371, 1307 cm^{-1}, which argues against a Rydberg assignment since these vibrational intervals do not match those of the asymptotic ion state which, from the HeI PES,[11] are 1495, 1473, 1425 and 1419 cm^{-1}. The vibrational intervals observed in the absorption spectrum correspond to the ν_3 mode frequency in the $2\,^1A'$ excited state. Its decrease with respect to $\nu_3 = 1777$ cm^{-1} in the ground state (Table 2) is consistent with our predictions based on the molecular orbital properties, as discussed in section 3.2.2. We remark that Bell *et al.*[22] give the absorption spectrum intervals as 1490, 1460, 1470 cm^{-1}, but their spectra are certainly less well resolved than ours and their measurements are not as secure for these diffuse bands on photographic plates, as can be surmised from their Figs. 1 and 2.

The $2\,^1A' \leftarrow 1\,^1A'$ assignment (Table 3) is confirmed by the transition strength, predicted to be strong.[19,35] Our absorption cross-section measurements give an oscillator strength $f \approx 0.2$, whereas Robin[38] gives $f = 0.37$, derived from the peak extinction coefficient reported by Barnes and Simpson.[40] These experimental values are considerably higher than the maximum value $f = 0.08$ expected for a 3s ← n′$_o$ Rydberg transition.[38] The shape of the generalized oscillator strength functions, as determined from EELS, is conjectured[18] to indicate important configuration interaction for this transition. Indeed, calculations show that in this valence transition there is a strong mixture of 3a″ ← 2a″ valence, 3pa′ ← 10a′ Rydberg and other single excitations.[35] The spatial extent of the nominal π* orbital, 3a″, given by $\langle r^2 \rangle^{1/2} = 8.7\ a_0$, is larger than that of a "normal" valence π* molecular orbital (3 a_0), but smaller than that of a 3da″ Rydberg MO (11.5 a_0).

We remark that in this 8.0–8.8 eV band system, the first band at around 65 400 cm^{-1} (our band 2, Table 1) remains distinct and is shifted only slightly to the violet along the isotopologue series HCOOH, HCOOD, DCOOH, DCOOD while the other bands seem to become more diffuse along the series and in DCOOH and DCOOD they merge into a continuum.[22] This may be a sign of increasing overlap of vibrational bands or of an increase in photodissociation rates. The latter would be unusual for deuteration of neutral states. We note that no fluorescence emission of parent or fragments is observed on excitation of formic acid in this spectral region.[12]

3.3.3. The 8.75–12.3 eV region bands. Many series of bands are observed in the 8.75–12.3 eV region (Figs. 4–6), some of which are valence bands and others Rydberg. We first classified some of these bands into 3 series, a,b,c; in addition there are some weaker bands that may also form series.

'a' series. This series (bands 7, 12, 18, 25 (Table 1, Fig. 4)), is identical to the C1 series of Bell *et al.*[22] The band intervals are 1509, 1476, 1460 cm^{-1} (Bell *et al.* 1509, 1479, 1476 cm^{-1}). The first two are similar to those of the ν_3 progression in the ion ground state, as determined from the photoelectron spectrum:[11] 1495, 1473, 1425 and 1419 cm^{-1}. It is therefore reasonable to assign this vibrational series to a Rydberg system that converges to the $1\,^2A'$ ground state of $HCOOH^+$. We note that the C1 series in DCOOD has intervals 1496, 1472, 1447 cm^{-1},[22] similar to the ground state ion values for DCOOD, 1472, 1474, 1424 cm^{-1},[11] thus confirming the Rydberg interpretation of the 'a' series. Tabayashi *et al.*,[14] as well as Suto *et al.*,[13] assign these bands to the 3p ← 10a′ Rydberg transition, without specifying which of the split core 3p levels is involved. Bell *et al.* assign the C1 series to the 3pa″ ← 10a′ Rydberg transition, on the basis that substructures in the profile of an (unspecified) band of the C1 system indicate that they correspond to out-of-plane A″ ← A′ transitions. However, no

structural constants were given and these substructures may be due to overlapping bands. Furthermore, a $3p'' \leftarrow 10a'$ transition is expected to be very weak.

We assign the 'a' series to the principal $3pa' \leftarrow 10a'$ Rydberg transition, whose first member has a quantum defect of $\delta = 0.66$. The second $3pa' \leftarrow 10a'$ transition, denoted as $3p'a' \leftarrow 10a'$ in Table 1 and in Fig. 4, we consider to correspond to the weak bands 13 and 19, whose frequency interval is 1484 cm^{-1}. The energy difference between the two $3pa' \leftarrow 10a'$ Rydberg transitions is 0.22 eV, is somewhat lower than the calculated value 0.46 eV.[35] The quantum defect of the $3p'a'$ level is $\delta = 0.55$.

The $3pa'' \leftarrow 10a'$ Rydberg transition bands should be weaker still and are not detected in our spectra. The weaker of the two $3pa' \leftarrow 10a'$ Rydberg transitions is expected to be quasi-degenerate in energy with a weak $3pa'' \leftarrow 10a'$ Rydberg band.[35]

Higher members of the $np \leftarrow 10a'$ Rydberg series are discussed later.

'b' series. This series is formed by bands 8, 14, 20, 27, 31 and 36 (Table 1, Fig. 4), the frequency intervals being 1492, 1427, 1372, 1314 and 1363 cm^{-1} respectively. It is identical to the C2 series of Bell *et al.*,[22] which has reported intervals of 1483, 1430, 1375 cm^{-1} (1482, 1456, 1415 cm^{-1} for DCOOD). (Each of the C1, C2 and C3 series of Bell *et al.* has a maximum of four reported members). Our 'b' series has frequency intervals reminiscent of the $2\,^1A' \leftarrow 1\,^1A'$ ($\pi^* \leftarrow \pi_2$) valence transition (1484, 1371, 1307 cm^{-1}) rather than those of the ion ground state so that we provisionally assign this series to a valence transition.

Although they are sharp, the 'b' series bands are not mentioned either by Suto *et al.*[13] or by Tabayashi *et al.*[14] No transition assignments of this series were given by Bell *et al.*[22] According to Robin,[44] there is a $\sigma^* \leftarrow n_o$ valence transition in this spectral region in formic acid so that the 'b' series may correspond to the $\sigma^* \leftarrow n_o$ valence transition, *i.e.* $4\,^1A' \leftarrow 1\,^1A'$ (Table 3). An alternative valence transition assignment is to $\pi^* \leftarrow \pi_1$, *i.e.* $3\,^1A' \leftarrow 1\,^1A'$, and this is discussed in more detail later. For both of these transitions we expect, as found, a decrease in the ν_3 frequency in the excited state as compared with the $1\,^1A'$ ground state.

'c' series. Sharp strong bands 9, 15, 21 and 28 (Table 1, Fig. 4) form the 'c' series, with frequency intervals 1452, 1419, 1363 cm^{-1}. They correspond to the C3 series of Bell *et al.*, which they assigned to a $3pa' \leftarrow 10a'$ Rydberg transition.[22] Their reported intervals are 1465, 1409 and 1407 cm^{-1}, whereas for DCOOD they are 1393, 1361 and 1338 cm^{-1}. The rather large frequency change with respect to HCOOH indicates that the vibrational mode excited in the upper state is not a pure carbon–oxygen vibration. These values are again reminiscent of valence transition intervals and we assign the 'c' series to a valence transition.

At this stage, we provisionally assign the 'b' series to $3\,^1A' \leftarrow 1\,^1A'$ ($\pi^* \leftarrow \pi_1$) and the 'c' series to $4\,^1A' \leftarrow 1\,^1A'$ ($\sigma^* \leftarrow n_o$) since several theoretical calculations involving (limited) configuration interaction[34,35] give the $\sigma^* \leftarrow n_o$ valence transition at higher energy than the $\pi^* \leftarrow \pi_1$ transition. In support of these assignments we note that the bands of the 'c' series have intensities that are a little greater than the corresponding bands of the 'b' series (Fig. 4, Table 1), which is qualitatively in agreement with calculations which predict an intensity ratio of the $4\,^1A' \leftarrow 1\,^1A'$ and $3\,^1A' \leftarrow 1\,^1A'$ transitions to be between 1.0 and 1.6.[37]

Before making our final assignments concerning the 'b' and 'c' series, we now discuss another possible assignment, *i.e.* that the 'b' and 'c' series belong to the same electronic transition with the interval between them being due to a vibration. Although this interval, of the order of 260 cm^{-1}, is much smaller than any vibrational frequency in the neutral ground state, we recall that the out-of-plane OH′ vibration drops from $\nu_9'' = 642$ cm^{-1} in the planar ground state to $\nu_9' = 251$ cm^{-1} in the non-planar $1\,^1A''$ state.[39] The structural and vibrational frequency changes in the $1\,^1A''$ state, with respect to the ground state, are in line with expectations from the respective bonding characteristics of the HOMO (10a′) and LUMO (3a″) orbitals, as discussed earlier. The tendency to non-planarity is associated with the 3a″ LUMO, so that this could also occur for the $3\,^1A'$ state where the excited electron is promoted to the 3a″ orbital.

Thus it is not impossible that the 'b' and 'c' series constitute two progressions in carbon–oxygen stretch vibrations, separated by $\nu_9' \approx 260$ cm^{-1} but both belonging to the $3\,^1A' \leftarrow 1\,^1A'$ transition. Excitation of ν_9' is consistent with an excited state that is out-of-plane, and therefore with a valence transition, since this vibration should be little excited in the planar Rydberg states of HCOOH. Assuming band 8 to be the origin band O_0^0 of the $3\,^1A' \leftarrow 1\,^1A'$ transition, the two progressions are as follows: bands 8, 14, 20, 27 form the progression 3_0^m; bands 9, 15, 21, 28 = $3_0^m 9_0^1$; bands 10, 16, 22, 29 = $3_0^m 9_0^2$; bands 11, 17, 23 = $3_0^m 9^3{}_0$, where $m = 0$–3.

However, if the 'b' and 'c' series are assigned to the transition, $3\,^1A' \leftarrow 1\,^1A'$, we must look for features corresponding to the $4\,^1A' \leftarrow 1\,^1A'$ transition, which is expected to have an intensity of the same order of magnitude as $3\,^1A' \leftarrow 1\,^1A'$. Robin[44] suggests that the $4\,^1A' \leftarrow 1\,^1A'$ transition corresponds to the underlying broad band in the 9 eV region, but from Fig. 4 it appears much more likely that the underlying feature is the tail of the strong $3\,^1A' \leftarrow 1\,^1A'$ transition. We therefore reject the assignment of the 'b' and 'c' series as belonging to a single transition and revert to their assignment as $3\,^1A' \leftarrow 1\,^1A'$ and $4\,^1A' \leftarrow 1\,^1A'$ respectively. This allows us to interpret bands 10, 16, 22 as being the vibronic transitions $3\,^1A' \leftarrow 1\,^1A'$ ($3_0^m 9_0^1$), $m = 0$–2 respectively, with $\nu'_9 \approx 365$ cm^{-1}, and bands 11, 17, 23 as the Rydberg bands (see later) $3pa' \leftarrow 10a'$ ($3_0^m 5_0^1$), $m = 0-2$ respectively, with $\nu'_5 \approx 1140$ cm^{-1}.

3.3.4. *ns* ← 10a′ Rydberg series. In section 3.3.1 we suggested that the broad 7.5 eV feature is probably mainly a diffuse $3sa' \leftarrow 10a'$ Rydberg band. Suto *et al.*[13] and Bell *et al.*[22] assign the next member ($n = 4$) of the *n*s series to a feature that corresponds to our band 41 at 9.94 eV (Table 1, Fig. 5), with band 47 forming a vibrational companion at 10.12 eV, *i.e.* at a vibrational interval of 1450 cm^{-1}. Our assignments are different. The $4sa' \leftarrow 10a'$ Rydberg transition is assigned to band 42, with band 49 as a $\nu'_3 = 1476$ cm^{-1} companion. The corresponding quantum defect is $\delta = 0.81$.

As discussed later, we have assigned band 41 to the Rydberg transition $3pa'' \leftarrow 2a''$ (O_0^0) and band 47 as $4sa' \leftarrow 10a'$ (6_0^1) (Table 1, Fig. 5). Tabayashi *et al.*[14] assigned band 41 as the second progression member of the $3p \leftarrow 2a''$ Rydberg transition and band 47 as the first member of the $4s \leftarrow 10a'$ Rydberg transition. As shown later, these are not justifiable assignments. In particular, they assign two progressions, of comparable intensity, to the $3p \leftarrow 2a''$ Rydberg transition, whereas on theoretical grounds we expect only one strong $3p'' \leftarrow 2a''$ transition, as well as two weak $3pa' \leftarrow 2a''$ transitions, as discussed in section 3.2.3. Furthermore, in their analysis of the $3p \leftarrow 2a''$ Rydberg progressions in the carbon–oxygen stretch vibration, the frequency intervals are much smaller than the value of ν_3 in the $1\,^2A''$ state of the ion[11] to which these Rydberg series converge.

Fridh,[19] on the basis of an EELS experiment, identified the $4sa' \leftarrow 10a'$ transition as being at about 9.65 eV, but reported no higher *n*s Rydberg transitions. This energy corresponds to our band 32 (Table 1) which was assigned by us, as well as by Tabayashi *et al.*,[14] as the first band in a progression of the Rydberg transition $3d \leftarrow 10a'$ (Fig. 4). Band 32 would give a quantum defect value $\delta = 1.14$ for the 4sa′ level. Using this δ value we predict the 5s Rydberg at 83 974 cm^{-1}. Indeed we observe a weak band 54 at 83 962 cm^{-1} (Fig. 5) but we assign

it as the first member of a 4d ← 10a′ progression: bands 54, 59, 65, *i.e.* the "D2" series of Bell *et al.*[22] In our assignments (Table 1), band 58 is the 5sa′ ← 10a′ transition, which gives $\delta = 0.85$ for the *n*s series), in good agreement with the analysis of Bell *et al.*

Indeed, $\delta = 0.85$ is much more satisfactory than $\delta = 1.14$ in interpreting the *n*s series. For example, calculation of the 6s Rydberg with $\delta = 1.14$, gives 86 695 cm^{-1} which would be in between bands 63 and 64 and is not obviously present. However, $\delta = 0.85$ gives 6s at 87 201 cm^{-1}, close to the sharp band 66 at 87 156 cm^{-1}, which corresponds to $\delta = 0.88$, and from which we can deduce a progression: bands 66, 70, 77 (intervals 1476, 1525 cm^{-1}). These bands were assigned by Tabayashi *et al.*[14] as part of the 3d ← 2a″ Rydberg transition, but their intervals are much too small for the CO vibration in the $1\,^2A''$ state of the ion, as will be discussed later.

Continuing the assignment of the *n*s series, a quantum defect of the order of 0.85 enables us to assign bands 69, 75 (interval 1436 cm^{-1}) to the 7s ← 10a′ Rydberg transition and band 72 to the 8s ← 10a′ Rydberg transition, with bands 79 ($\nu'_3 = 1516$ cm^{-1}, but this band appears to have two components), and band 78 ($\nu'_6 = 1194$ cm^{-1}) as vibrational companions.

3.3.5. The *n*p ← 10a′ Rydberg series. In section 3.3.3 we assigned the 'a' series as the principal of the two possible 3pa′ ← 10a′ Rydberg transitions. This provides a quantum defect value of $\delta = 0.66$, which is very reasonable for an *n*p Rydberg series. We now examine higher members of the *n*p series using δ values of this order of magnitude.

The 4pa′ ← 10a′ Rydberg transition origin is assigned to band 48 (Table 1, Fig. 5), which corresponds to $\delta = 0.60$. The very weak band 53 at 83 680 cm^{-1} is assigned to the analogous weak 4p′a′ ← 10a′ Rydberg transition. Its low effective quantum defect, $\delta = 0.22$, might seem to make this assignment improbable but we note that the calculated quantum defect[35] is sharply reduced by a factor ≈2 in going from 4pa′ to 4p′a′, and that our observed energy difference between these two levels, 0.18 eV, is close to the calculated value, 0.21 eV. We remark that band 48 is also assigned by Bell *et al.*[22] as 4p. We assign bands 52, 57 (Bell F1 series) to the 4pa′ ← 10a′ (3_0^m), $m = 1$ and $m = 2$ transitions, and bands 51, 56, 61 as involving the additional excitation of ν'_6 (Table 1).

In all, we have assigned *n*pa′ ← 10a′ Rydberg transitions, and their companion bands, form $n = 3$–9, and for which the quantum defects are essentially in the range 0.59–0.66 (Table 1). Weak *n*p′a′ ← 10a′ Rydberg transitions were assigned, as discussed above, only for $n = 3$ and $n = 4$. Our *n*pa′ ← 10a′ assignments are largely in agreement with those of Bell *et al.*,[22] and differ totally from those of Tabayashi *et al.*[14] Further objections to absorption band assignments of Tabayashi *et al.*, in particular concerning Rydberg transitions converging to the first excited state of the formic acid ion, will be presented below.

3.3.6. The *n*da′ ← 10a′ Rydberg series. Although for each value of *n*, there are expected three *n*da′ ← 10a′ transitions, it is probable that one of these transitions has the major oscillator strength. In any case, we do not observe more than one *n*da′ ← 10a′ transition for each value of *n*. Our assignments in Table 1 of the origin bands and companion bands of this Rydberg series basically agree with that of Bell *et al.*:[22] 3d: bands 32, 38, 43; 4d: bands 54, 59, 65; 5d: bands 64, 69 (Table 1, Figs. 4 and 5). The corresponding δ values of the origin bands are given in Table 1.

3.3.7. Vibrational frequencies of the Rydberg states converging to the ground state of the formic acid ion. Two carbon–oxygen stretch vibrational modes, ν_6 and ν_3 were excited in the Rydberg levels, giving rise to the companion bands discussed above. The average values of the frequencies over all companion bands in the *n*s, *n*p and *n*d Rydberg series converging to the ground state of the ion are $\nu_6 = 1178$ cm^{-1} and $\nu_3 = 1477$ cm^{-1}. These values are very close to, and within the error limits of, the frequencies of these modes in the ion ground state, $\nu_6 = 1196$ cm^{-1} and $\nu_3 = 1495$ cm^{-1} established by photoelectron spectroscopy.[11] The ν_5 mode was assigned in some of the 3pa′ ← 10a′ transition bands, yielding a frequency $\nu_5 \approx 1140$ cm^{-1}. This vibrational mode is unresolved from that of mode 6 in the He I PES of the ion ground state of HCOOH[11b] (*cf.* Table 2).

3.4. Spectral assignments: Rydberg transitions converging to the first excited ion state $1\,^2A''$

Assignments of Rydberg bands converging to the first excited electronic state, $1\,^2A''$, of the formic acid ion have not previously been reported except by Tabayashi *et al.*[14] who assigned two 3p ← 2a″ and one 3d ← 2a″ progressions. In section 3.3.4 we have discussed our objections to their 3d ← 2a″ progression analysis and present below our reasons for rejecting their assignments of the 3p ← 2a″ Rydberg transitions. This turns in part on the incorrect assumption of Tabayashi *et al.* that the carbon–oxygen stretch vibration has a similar frequency in the Rydberg states converging to the ground and to the first excited state of the ion.

In searching for Rydberg bands converging to the $1\,^2A''$ state of $HCOOH^+$ we started with the following two criteria:

(1) We expect to find an energy interval ΔE of the order of 8500 cm^{-1} between the *n*s, *n*p and *n*d Rydberg transition bands converging to the ground state of the ion and the corresponding series of bands which converge to the first excited state, since this is the value of the difference in the energies of these two ion states.[11]

(2) The existence of companion bands to the Rydberg transition O_0^0 band at intervals similar to those of vibrational frequencies of the first excited ion state as given in Table 2.

These criteria helped us to establish the following assignments.

3.4.1. *n*sa′ ← 2a″ Rydberg series. The *n*sa′ ← 2a″ Rydberg series bands correspond to out-of-plane $1\,A'' \leftarrow X\,^1A'$ transitions, so they are not expected to be very intense. Demoulin[35] calculates the 3sa′ ← 2a″ band to be at 8.67 eV and 4sa′ ← 2a″ at 10.86 eV. The calculated differences $\Delta E'$ between the *n*sa′ ← 10a′ and the corresponding *n*sa′ ← 2a″ transitions are $\Delta E' = 0.53$ eV ($n = 3$) and $\Delta E' = 0.86$ eV ($n = 4$). It is difficult to compare the experimental value of $\Delta E'$ for $n = 3$, because of the broadness of the 3sa′ band in both series; an approximate value is $\Delta E' = 1.0 \pm 0.4$ eV for $n = 3$ (see below). However, a more precise value, $\Delta E' = 0.87$ eV, very close to the calculated value,[35] is obtained for $n = 4$. These theoretical and experimental values are less than the experimental $\Delta E = 1.05$ eV between the ion limit states, but the fact that there is an increase in going from $n = 3$ to $n = 4$, at least in the calculated values, is not surprising since it is usual for the Rydberg level properties to approximate closer to the ion as principal quantum number *n* increases.

We assign in Table 1 the following members of the *n*sa′ ← 2a″ series:

4s, to band 67 at 87 591 cm^{-1} (Fig. 5); band 70 at 88 632 cm^{-1} in part to a $\nu_6 = 1040$ cm^{-1} companion; band 76 at 89 914 cm^{-1} may include a possible $\nu_3 = 2323$ cm^{-1} companion.

5s, to band 90 at 92 729 cm^{-1} (Fig. 6); band 92 is its $\nu_6 = 1057$ cm^{-1} companion; and possibly band 95 contains the $\nu_3 = 2291$ cm^{-1} companion.

6s, to band 98 at 95 415 cm^{-1}; band 106 contains the $\nu_3 = 2307$ cm^{-1} companion; band 101 at 96 447 cm^{-1} is the $\nu_6 = 1026$ cm^{-1} companion.

7s, to band 102 at 96 689 cm^{-1}; band 106 contains also the $\nu_6 = 1033$ cm^{-1} companion, and band 109 possibly the ν_3 companion.

8s, to band 105 at 97 544 cm^{-1}; band 108 at 98 568 cm^{-1} is the $\nu_6 = 1024$ cm^{-1} companion.

Using $\delta = 1.05$, we predict 3sa′ at 70 978 cm^{-1}. This might correspond to part of the high frequency tail of the broad feature between bands 5 and 7 (Figs. 3, 4). As mentioned above, we expect it to be broad, since a 3s Rydberg level is involved.

The average value of δ is 1.05 for the *n*sa′ ← 2a″ series, which is very reasonable for an *n*s Rydberg series. We note that Demoulin[35] predicts $\delta = 1.12$ for the 4sa′ level, based on IE = 12.50 eV for the first excited ion state, whereas our experimental value, used for determining δ, is IE = 12.3783 eV.[11]

3.4.2. *n*p ← 2a″ Rydberg series. As discussed earlier, on symmetry grounds one expects only one strong 3p ← 2a″ transition, *i.e.* 3pa″ ← 2a″. We assign band 41 (Table 1, Fig. 5) to the origin band of this transition, giving $\delta = 0.64$, with band 45 as $\nu_6 = 1041$ cm^{-1} companion, band 46 as $\nu_5 = 1162$ cm^{-1} companion, and the broad band 50 (Table 1, Fig. 5), which obviously has overlapping features, as containing a ν_3 companion. The higher members of this Rydberg series are assigned as follows:

4pa″: assigned to band 76 at 89 914 cm^{-1} (Table 1, Fig. 6).

5pa″: assigned to band 93 at 93 963 cm^{-1}, with band 95 as $\nu_6 = 1057$ cm^{-1} companion, and band 100 as $\nu_3 = 2387$ cm^{-1} companion.

6pa″: assigned to band 99 at 95 923 cm^{-1}, with band 103 partially as $\nu_6 = 1073$ cm^{-1} companion.

7pa″: assigned as band 103 at 96 996 cm^{-1}, with band 107 as $\nu_6 = 1072$ cm^{-1} companion.

We assign also some members of a weaker 3p ← 2a″ transition, *i.e.* 3pa′ ← 2a″, to bands 35 (origin band), band 40 ($\nu_6 = 1033$ cm^{-1} companion), band 44 ($\nu_3 = 2339$ cm^{-1} companion). In agreement with these assignments, the relative intensities of bands 35, 40 and 44 (Table 1, Fig. 5) are very similar to those of the O_0^0, 6_0^1 and 3_0^1 photoelectron bands corresponding to ionization to the first excited state of HCOOH.[11] Higher members of the *n*pa′ ← 2a′ Rydberg series were not observed.

Band 40 has been assigned by Tabayashi *et al.*[14] as the first band of a 3p ← 2a″ transition vibrational progression corresponding to our bands 40, 45, 50, 55. They assigned also a second, similarly strong 3p ← 2a″ vibrational progression, corresponding to our bands 35 (or 36), 41, 46, 52. However, as discussed above, on symmetry grounds one expects only one intense 3p ← 2a″ transition, *i.e.* 3pa″ ← 2a″. This argues strongly against the 3p ← 2a″ Rydberg transition assignments of Tabayashi *et al.*

3.4.3. *n*d ← 2a″ Rydberg series. Although, in theory, there are two *n*da″ ← 2a″ transitions and three *n*da′ ← 2a″ transitions for each value of *n*, the latter three being out-of-plane transitions, only one, short, *n*da″ ← 2a″ series was observed. Demoulin[35] calculates that even this in-plane transition series will be weak. Our band assignments are as follows:

3d: we assigned band 63 at 86 438 cm^{-1} (Table 1) as being due in part to the 3da″ ← 2a″ transition. Vibrational companion bands may exist as unresolved shoulders of higher energy bands, *e.g.* band 71 as the ν_3 companion.

4d: assigned as part of band 88, with band 94, which appears to have two components, as its ν_3 companion.

5d: assigned as band 96 at 95 133 cm^{-1}.

3.4.4. Vibrational frequencies of Rydberg levels converging to the ion first excited state. In the *n*s, *n*p and *n*d Rydberg series converging to the first excited state $1\,^2A''$ of the formic acid ion we observed companion bands corresponding to the excitation of the vibrational modes ν_3 and ν_6. The average values of the vibrational mode frequencies are $\nu_3 = 2344$ cm^{-1} and $\nu_6 = 1044$ cm^{-1}. These values are very close to, and within the error limits of, the frequencies of these modes in the first excited state of the ion, $\nu_3 = 2343$ cm^{-1} and $\nu_6 = 1029$ cm^{-1} (Table 2), as measured in photoelectron spectra.[11] There is also one value for mode 5, $\nu_5 = 1162$ cm^{-1}, for 3pa″, derived from band 46, whereas we expect about 1300 cm^{-1} from the He I PES analysis.[11] However, this absorption band was measured as a shoulder to band 45 (Fig. 5), so that the derived ν_5 value is uncertain.

4. Absorption at higher energies: 12.3–22 eV

The absorption spectra above the second ionization energy are shown in Figs. 1 and 7. There are no previous reports concerning absorption spectra of formic acid in the 12.3–22 eV region but there are published EELS spectra, up to 15.05 eV [19] and to 16 eV,[20] whose energy resolution is very much less than that of our absorption spectra. Both EELs spectra show a broad feature between 13 and 15 eV peaking in the 14.2 eV region. Our absorption spectrum shows a broad feature between 12.8 and 15.2 eV (Fig. 1) which contains a shoulder at about 13.5 eV (Fig. 7, band 110), also evident in Fridh's EEL spectrum,[19] and some not well resolved structure in the 14–15 eV region, with an intensity maximum at about 14.5 eV. At higher energies we observe a series of absorption bands (114–123, Table 1) in the 15.7–16.8 eV region superimposed on rising broad background whose maximum intensity is at 17.9 eV (Fig. 1), followed by a shallow minimum at about 18.9 eV and a fairly constant intensity absorption between 20 and 22 eV.

In order to analyse the absorption spectra observed between 12.3 and 22 eV region we first discuss the ion states in this region, which should be the limit states to which Rydberg series in this spectral region converge. Photoelectron spectroscopy has established a series of ion states arising by successive loss of an electron from molecular orbitals of HCOOH:

$\ldots(6a')^2(7a')^2(8a')^2(1a'')^2(9a')^2(2a'')^2(10a')^2$.

In the 12.3–22 eV region there are ionization limits corresponding to loss respectively of the 9a′, 1a″, 8a′ and 7a′ electrons in one electron transitions. Loss of the 6a′ electron is calculated to take place at an energy about 4.5 eV above that of the 7a′ electron,[34,37] which is in the 17.5–17.7 eV region.[11b,15] Therefore ionization of a 6a′ electron can be estimated to occur at about 21.5 eV, so that absorption in the 18–22 eV region may be Rydberg bands converging to the $6a'^{-1}$ ion state, *i.e.* $5\,^2A'$ (see below). We neglect any satellite states corresponding to two-electron transitions and configurational effects in general, which is reasonable for HCOOH below 22 eV.[45] States which are associated with loss of the inner valence electrons 5a′ and 4a′ give rise to many satellite bands whose intensities are distributed over the 30–40 eV region in high energy PES.[45,46] We now examine the absorption spectra in this context, searching for Rydberg bands converging to the various ionization limits between 12.3 and 22 eV.

4.1. Promotion of a 9a′ electron: *n*(s,p,d) ← 9a′; limit ion state $2\,^2A'$

The He I PES shows a broad band in the 14.2–15.3 eV region, peaking at 14.81 eV, corresponding to loss of a 9a′ electron and formation of the $2\,^2A'$ ion state.[11b] The broad absorption band between 12.8 and 15.2 eV (Fig. 7) may therefore correspond to a set of broad overlapping Rydberg bands and their companion bands converging to the $2\,^2A'$ ion state whose adiabatic IE is at about 14.15 eV and whose vertical IE is at 14.81 eV.[11b]

Demoulin,[35] using 14.7 eV as the value of the vertical IE of the 9a′ electron calculates the 3sa′ ← 9a′ transition to be at 11.24 eV = 90 656 cm^{-1}, with $\delta = 1.017$. There is a broad background absorption in the 11–13 eV region underlying sharp well resolved features (Figs. 1 and 6). This broad background could contain broad overlapping 3s, 3p and 3d Rydberg bands and their companion bands, converging to the $2\,^2A'$ ion state.

Using our experimental IE (v) and a value $\delta = 0.85$ similar to that in ns Rydbergs converging to the ion ground state, we predict the 3s ← 9a′ Rydberg transition to occur at 90 387 cm^{-1} = 11.207 eV. However, it is physically more satisfying to calculate the Rydberg transitions on the basis of the adiabatic IEs, and to estimate the most intense Franck–Condon transition by adding the difference between the adiabatic and vertical IEs. We thus predict the 4s origin band to be at 103 067 cm^{-1} = 12.779 eV, which is in a region of featureless absorption. The most intense Franck–Condon transition is estimated to be 0.66 eV higher than the calculated origin transitions, *i.e.* at 108 390 cm^{-1}. This would be in the neighbourhood of the shoulder band 110 at 108 723 cm^{-1} in a region of quasi-continuous absorption (Fig. 7).

Turning now to the np ← 9a′ Rydberg transitions, we assign the 3pa′ ← 9a′ transition to band 91 at 93 003 cm^{-1}, corresponding to $\delta = 0.72$. There are ν_3 and $2\nu_3$ vibrational companions at, respectively, bands 94 and 99 (Table 1). With $\delta = 0.72$, the 4pa′ ← 9a′ transition would be at 103 931 cm^{-1} = 12.886 eV, a region of weak absorption (Figs. 1 and 7), and the most intense Franck–Condon transition at 109 373 cm^{-1} = 13.546 eV, *i.e.* in the 110 shoulder band region. The 5p and 6p bands are calculated to occur in the broad band region between 14 and 14.4 eV and may correspond to poorly resolved features in this region.

We did not search for nd ← 9a′ Rydberg transitions.

4.2. Promotion of a 1a″ electron: n(s,p,d) ← 1a″; limit ion state $2\,^2A''$

The vertical IE = 15.75 eV for forming the $2\,^2A''$ state, while the adiabatic IE ≈ 15.35 eV.[11b] On symmetry grounds, the only strong Rydberg transitions converging to this ion state are expected to be $n$pa″ ← 1a″and $n$da″ ← 1a″. We considered whether some barely resolved absorption features in the 14.5–15 eV region (Fig. 7) may be due to Rydberg bands converging to the $1a''^{-1}$ ion state $2\,^2A''$. There are at least four (broad) features in this region, with an average band interval ≈1345 cm^{-1}. In the He I PES of HCOOH we find, between 15–15.5 eV, bands with an interval of the order of 1290 cm^{-1}, but these are vibrational components of the lower-lying $2\,^2A'$ ion state. The $2\,^2A''$ state vibrational intervals are of the order of 970 cm^{-1},[11b] which are much smaller than the ≈1345 cm^{-1} absorption band intervals. This indicates that the absorption features in the 14.5–15 eV regions are not associated with Rydberg transitions leading to the $2\,^2A''$ ion state. They may belong to high-lying valence transitions, as yet unrecognised, *e.g.* $3\,^2A'' \leftarrow 1\,^2A'$, corresponding to 11a′ ← 2a″ or $4\,^2A'' \leftarrow 1\,^2A'$ (11a′ ← 1a″), which are expected to be weak, or to the stronger, in-plane, transitions $5\,^2A' \leftarrow 1\,^2A'$ (11a′ ← 9a′) and $6\,^2A' \leftarrow 1\,^2A'$ (11a′ ← 8a′).

4.3. Promotion of a 8a′ electron: n(s, p, d) ← 8a′; limit ion state $3\,^2A'$

Loss of a 8a′ electron gives rise to the $3\,^2A'$ state whose adiabatic IE = 16.971 eV. The He I PES shows well defined photoelectron vibrational bands in this region.[11b,15] We considered whether the sharp absorption features, bands 114–123, (15.75–16.73 eV, Fig. 7), are Rydberg bands converging to the $3\,^2A'$ ion state. These bands have as successive intervals 1307, 1259, 1304, 1298, 1380, 1322 cm^{-1}, with possibly some side-bands. Measurement of the PES in the 17 eV region[11b] shows that the main bands have successive intervals of 1307, 1267, 907, 956, cm^{-1}, and that there are several much weaker bands. A direct comparison between the absorption in the 15–17 eV region and the He I PES in the 17 eV region shifted down by 1.2223 eV is given in Fig. 8. It clearly shows excellent correspondence between the two spectra in the 15.75–16.06 eV (absorption) region, *i.e.* over the first two band intervals, but considerable difference at higher energies, *i.e.* above 16.06 eV in the absorption spectrum and 17.28 eV in the He I PES. In the PES, this is the region usually assigned to the $4\,^2A'$ ion state resulting from loss of a 7a′ electron.[11b,15,47]

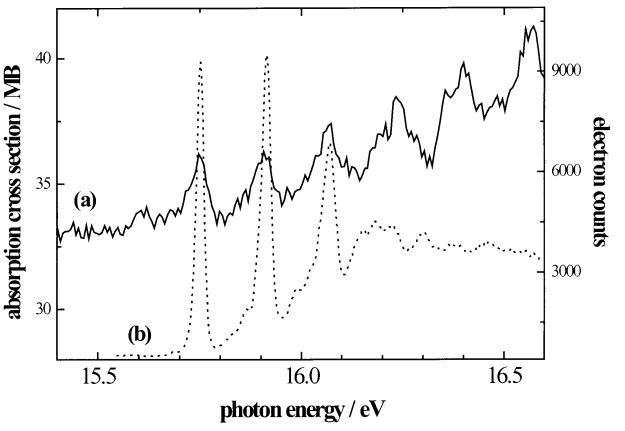

Fig. 8 (a) HCOOH absorption spectrum 15.4–16.6 eV; (b) He I photoelectron spectrum in the 17 eV region[11b] red shifted by 1.2223 eV.

We therefore assign bands 114–123 as associated with Rydberg levels converging to the $3\,^2A'$ ion state. The bands form an apparent vibrational progression whose interval is about 1300 cm^{-1}. This is investigated further below. We now examine specific Rydberg transitions converging to the $3\,^2A'$ state of the ion.

4.3.1. $n$sa′ ← 8a′ series. No satisfactory assignments were made for the $n$sa′ ← 8a′ Rydberg bands using three different values $\delta = 0.8$, 0.9 and 1.0. Although a few bands could be fitted for each value of δ, the key 4s and 5s bands could not be assigned satisfactorily. We conclude that there is no clear evidence for the ns series. However, since the nd series could be assigned using δ values of the order of 0.125 (see later), it is not impossible that the ns series exists with a value $\delta \approx 1.125$. This remains to be further explored.

4.3.2. $n$pa′ ← 8a′ series. The $3\,^2A'$ ion state is at 16.971 eV = 136 880 cm^{-1}.[11b] Taking band 114 at 126 999 cm^{-1} as O_0^0 origin band provides an $n - \delta$ value of 3.334. It therefore is reasonable to assign band 114 (Table 1, Fig. 7) as 4pa′ ← 8a′, ′, with $\delta = 0.67$. Bands 115 and 116 (in part, see later) can be assigned as vibrational components to the 4pa′ ← 8a′ transition, with a vibrational frequency of ≈1300 cm^{-1}, which is a value corresponding to ν_6 in the $3\,^2A'$ ion state.[11b]

Other $n$pa′ ← 8a′ transitions are assigned as follows. The broad feature band 111 can be assigned to the 3pa′ ← 8a′ transition, giving $\delta = 0.67$, the 5pa′ ← 8a′ transition to band 117 ($\delta = 0.69$), with band 118 being reasonably assigned as being, in part (see below), its ν_6 companion band ($\delta\nu = 1298$ cm^{-1}). The 6pa′ ← 8a′ transition is assigned to the weak feature 119 at ≈132 919 cm^{-1} (16.48 eV) corresponding to a value of $\delta = 0.74$. Another weak feature 121 at ≈16.624 eV = 134 081 cm^{-1} and this is assigned to the 7pa′ ← 8a′ transition, with $\delta = 0.74$. Using $\delta = 0.74$, the 8pa′ ← 8a′ transition is calculated to be at 134 798 cm^{-1} = 16.713 eV, which is within the profile of band 123 whose maximum intensity is at 134 968 cm^{-1}.

***n*da′ ← 8a′ series.** From its relative intensity and profile, we consider that band 116, apart from its 4p vibrational component (see above), also contains the 4da′ ← 8a′ transition band, with $\delta = 0.125$. The 5da′ ← 8a′ transition is assigned to band 118 at 132 266 cm^{-1} (Fig. 7), with $\delta = 0.124$. As mentioned above, this band also probably contains the ν_6 companion band of the 5pa′ ← 8a′ Rydberg transition band 117. The 6da′ ← 8a′ transition is assigned to band 120 at 133 645 cm^{-1} (Fig. 7), with $\delta = 0.17$, while the 7da′ ← 8a′ transition can be assigned to band 122 at 16.682 eV = 134 549 cm^{-1}, with $\delta = 0.14$.

4.3.3. Relation of bands 114–123 to the photophysics of formic acid. It is remarkable that the absorption bands 114–123 in the 15.7–16.8 eV region appear as features in the ion quantum yield ϕ_i curve,[12] as illustrated in Fig. 9, whereas most of the rest of the ϕ_i curve is continuous, reaching an ion quantum yield of unity at 18.0 ± 0.1 eV.[12] This behaviour indicates that the bands 114–123 Rydberg levels which converge to the $3\,^2A'$ ion state undergo autoionization on a relatively long timescale. To determine the autoionization rate we measured the FWHM of the ϕ_i and the absorption curve peaks above their respective background continua in the 15.7–16.8 eV region and compared them respectively with the energy resolutions of the ion quantum yield (50 meV) and absorption (10 meV in the 16 eV region) measurements. The ϕ_i and the absorption peaks were both found to have FWHM values of about 50 meV. From this we infer that the autoionization rate $k_{ai} \approx 7.5 \times 10^{13}$ s^{-1} since the absorption peak FWHM is much greater than the absorption spectral resolution.

The Rydberg states converging to the $3\,^2A'$ state have this ion state as their core. The fact that these absorption bands are sharp, and the existence of well resolved vibrational structure of the $3\,^2A'$ ion state in the He I PES, indicate that this ion state has a relatively long lifetime. A photoelectron–photoion coincidence (PEPICO) study by Nishimura *et al.*[48] of the breakdown curves of HCOOH up to 19 eV bears on this question and brings up some interesting photophysical aspects. The results of their study of the fragment ions $COOH^+$ and HCO^+ led them to suggest that formic acid excited to the $3\,^2A'$ state of $HCOOH^+$, can relax radiatively to the first excited ion state $1\,^2A''$ which then dissociates to $H + COOH^+$. We have estimated that the expected emission should occur at $\lambda \approx 282$ nm.[12]

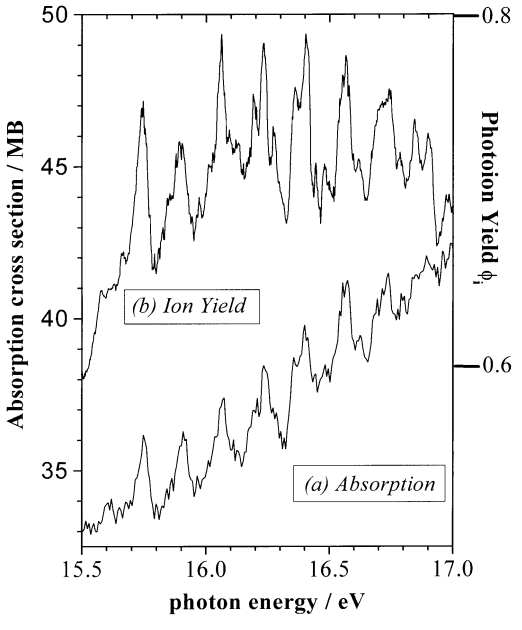

Fig. 9 (a) HCOOH absorption spectrum 15.5–17.0 eV; (b) photoion quantum yield curve in the 15.5–17.0 eV region.[12]

However, this is in a spectral region where relatively strong OH emission is observed on photon excitation to the $3\,^2A'$ state of $HCOOH^+$,[12] thus making it difficult to verify the proposed fluorescence mechanism. This is discussed in more detail elsewhere.[12]

We propose an explanation for another aspect of the observed breakdown curve. In Fig. 2b of Nishimura *et al.*,[48] the increase in the $COOH^+$ signal begins at about 15.8 eV, rising to about 17.3 eV then drops sharply at higher energies. We propose that the increasing $COOH^+$ signal is produced by dissociative autoionization from the Rydberg levels leading to $3\,^2A'$, and decreases when excitation to the $4\,^2A'$ state becomes important at the Franck–Condon maximum at about 17.3 eV (see later). The mirror image behaviour of the energy dependence of the formation of HCO^+ shows that the two channels are competitive. The breakdown curves indicate that the yield ratio between the $H + COOH^+$ and the $OH + HCO^+$ dissociative autoionization channels increases with increasing energy in the 15.8–17.3 eV region. A study of the breakdown curves of formic acid at an adequate high spectral resolution is necessary in order confirm our proposed dissociative autoionization interpretation.

4.4. Promotion of a 7a′ electron: *n*(s,p,d) ← 7a′; limit ion state $4\,^2A'$

The precise energy of the $4\,^2A'$ state resulting from loss of a 7a′ electron has been difficult to establish from the experimental viewpoint.[15,16,47] In the past, the $4\,^2A'$ state was assumed to occur in the energy region where there is a modification in the regularity of the PES vibrational bands initially belonging to the $3\,^2A'$ state, *i.e.* around 17.28 eV.[11b,15,16,47] From a study of the He I PES of the four isotopologues HCOOH, HCOOD, DCOOH and DCOOD,[11b] it has recently been established that the origin of the $4\,^2A'$ state of $HCOOH^+$ corresponds to a very weak PES band at 16.9084 eV, *i.e.* slightly below that of the strong PES band origin of the $3\,^2A'$ state which is at 16.9738 eV. The displaced oscillator structure of transitions to the $4\,^2A'$ state[11b] made it difficult for us to assign specific Rydberg transitions converging to this ion state. Nevertheless, we can state that the principal transitions should occur in the 16–17.5 eV region and may be responsible for the underlying increase of absorption intensity in this spectral region (Fig. 7).

4.5. Promotion of a 6a′ electron: *n*(s,p,d) ← 6a′; limit ion state $5\,^2A'$

As mentioned earlier, the loss of the 6a′ electron is expected to occur close to or above 22 eV. In the He II PES there is indeed a broad band between 21 and 23 eV, maximum at 22 eV, showing no marked signs of vibrational structure.[46,49] The broad absorption in the 17.5–22 eV region may therefore correspond to unresolved Rydberg bands converging to the $5\,^2A'$ state. Although there are undulations in the absorption curve between 18 and 22 eV (Fig. 1), no other distinct features are observed in this spectral region.

5. Quantum defect values

The orders of magnitude of the δ values of the s, p and d levels reported in Table 1 are as expected for normal molecules.[38,44] The uncertainity in the quantum defect values increases with increasing principal quantum number, as the density of absorption bands increases on approaching the Rydberg asymptote and the energy difference between ionization energy and term value becomes more exacting in determining the δ values. It is clear, however, that the quantum defect values for the *n*sa′ ← 10a′ transitions (4s: 0.81, 5s: 0.85, 6s: 0.88,...) are significantly smaller than those of the corresponding

$n$sa′ ← 2a″ transitions (4s: 1.01, 5s: 1.07, 6s: 1.02, ...), indicating a difference in molecular core penetration in these two cases. This is also true, to a less marked extent, for the $n$pa′ ← 10a′ (3p: 0.66, 4p: 0.60, 5p: 0.60, 6p: 0.59,...) and $n$pa″ ← 2a″ transitions (3p: 0.64, 4p: 0.67, 5p: 0.68, 6p: 0.70, ...), whereas the values for the $n$pa″ ← 2a″ and $n$pa′ ← 8a′ (3p: 0.67, 4p: 0.67, 5p: 0.69, 6p: 0.74, ...) transitions are very similar. Table 1 also includes the quantum defect values for the 3p′a′ ($\delta = 0.55$) and 4p′a′ ($\delta = 0.22$) levels of the np′a′ ← 10a′ Rydberg series, which are lower than for the corresponding principal 3pa′ and 4pa′ levels, in agreement with model calculations, as discussed in sections 3.3.3 and 3.3.5. No marked differences are found between the quantum defect values for the nd levels of the $n$da′ ← 10a′, $n$da″ ← 2a″ and $n$da″ ← 8a′ transitions, which have similar δ values, of the order of 0.15 (Table 1).

6. Conclusion

Absorption spectra of HCOOH were measured between 6 and 22 eV at an equivalent resolution to the best previously achieved over a much more limited spectral range[13,14,22] (5–11.7 eV). In the spectral region common to previous measurements, we observed and assigned many features seen by Bell *et al.*[22] but unassigned by these authors. Many other spectral features not reported by Bell *et al.*, but evident in other published absorption spectra below 11.7 eV,[13,14] were also observed in our spectra.

In our analysis of the absorption spectra we discuss and use the molecular orbital structure of formic acid, the associated bonding properties, and the relevant theoretical calculations on valence and Rydberg states of formic acid. Data on ionic states and their structural and dynamic properties, obtained from He I photoelectron spectroscopy of formic acid[11] were also used. Five valence transitions and the different types of expected Rydberg transitions converging to the ground state $1\,^2A'$ and the first excited electronic state $1\,^2A''$ of the formic acid ion were first discussed. The corresponding valence and Rydberg absorption bands were then assigned in the spectral region below 12.3 eV.

Our analyses disagree in considerable part with the assignments of Bell *et al.*[22] (adopted also by Suto *et al.*[13]) in the region below 10.15 eV. In particular, we recognise and assign the valence transitions $2\,^1A' \leftarrow 1\,^1A'$ ($\pi^* \leftarrow \pi_2$), $3\,^1A' \leftarrow 1\,^1A'$ ($\pi^* \leftarrow \pi_1$) and $4\,^1A' \leftarrow 1\,^1A'$ ($\sigma^* \leftarrow n_o$). The experimental energies of these valence transitions are systematically smaller than the quantum chemically calculated values (Table 3), illustrating insufficiencies of the latter, in particular concerning adequate configuration interaction.

Concerning the Rydberg transitions converging to the ground state of the ion, we disagree with some of the Bell *et al.* assignments for the $n$sa′ ← 10a′ series, as well as those of Tabayashi *et al.*[14] which were limited to 4sa′ ← 10a′ for this series, and we provide different band assignments for these transitions. In general, there is good agreement between our assignments and those of Bell *et al.*[22] for the np ← 10a′ series for $n \geqslant 4$, *i.e.* between 10.15 and 11.33 eV. Our assignments differ in part from those of Tabayashi *et al.*[14] for the 3pa′ ← 10a′ transition (which was the only member of the np ← 10a′ series reported by these authors). In particular, we show that there is only one strong component, and not two as assigned by Tabayashi *et al.* for this transition. However, our assignments for the nd ← 10a′ series agree well with those of Bell *et al.*[22] and of Tabayashi *et al.*[14] for particular bands of this series. Associated with several of the ns,np,nd ← 10a′ Rydberg bands are companion bands corresponding to excitation of ν_6 and ν_3 mode vibrations; their frequencies correspond well to those known, from photoelectron spectroscopy, for the $1\,^2A'$ ground state of the formic acid ion.

The only previous assignment of Rydberg bands converging to the first excited electronic state, $1\,^2A''$, of the formic acid ion was carried out by Tabayashi *et al.*[22] We strongly disagree with their assignments. Our analysis and assignments of these transitions is based on a better knowledge of the ionization limit and of the $1\,^2A''$ ion state vibrational frequencies which, in turn, result from a recent He I photoelectron spectroscopic study of formic acid isotopologues.[11b] The assignments also take into account the relative intensities of Rydberg transitions expected on electronic state symmetry grounds. A large number of absorption bands corresponding to $n$sa′ ← 2a″, np ← 2a″ ″ and 3da″ ← 2a″ Rydberg transitions were assigned, including ν_3 and ν_6 vibrational components whose frequencies agree well with those of the $1\,^2A''$ ion state.

Entirely novel aspects of our study concern the observation, analysis and assignment of absorption features at higher energies, between 12 and 22 eV, carried out here for the first time. The existence of Rydberg bands was explored for transitions whose limiting ion states are respectively $2\,^2A'$, $2\,^2A''$, $3\,^2A'$, $4\,^2A'$ and $5\,^2A'$, corresponding to ionization of electrons from the successive molecular orbitals 9a′, 1a″, 8a′, 7a′ and 6a′. Rydberg bands converging to these ionization limits were not observed as discrete features, except for the $2\,^2A'$ ($9a'^{-1}$) and $3\,^2A'$ ($8a'^{-1}$) cases. The Rydberg bands converging to the other ionization limits are apparently broad and merge to form the broad features or underlying continuous absorption observed in specified high energy regions.

In particular, assignments were made for $n$pa′ ← 8a′ and $n$da′ ← 8a′ Rydberg transitions, which exhibit relatively narrow discrete absorption bands. A comparison between absorption features and similar features observed in the ion quantum yield curve[12] in the 15.7–16.8 eV region showed that these Rydberg states undergo autoionization with a rate $k_{ai} \approx 7.5 \times 10^{13}$ s^{-1}. This is a spectral region where PEPICO measurements on formic acid[48] indicate the existence of two competitive dissociation channels, respectively to $H + COOH^+$ and $OH + HCO^+$. In a novel interpretation of the observed breakdown curve behaviour of formic acid we have proposed that the fragmentation in this energy region results from dissociative autoionization.

The detailed information obtained in the present absorption study is of direct use not only in the interpretation of formic acid dissociative photoionization but also for other photophysical properties, such as fluorescence emission observed from neutral and ionic dissociation channels as a function of excitation energy.[12] As mentioned in the Introduction, this information is of direct interest for certain types of astrophysical and exobiology studies, and will be exploited elsewhere.

Acknowledgements

This work has been supported by the TMR programme of the European Union under contract FMRX-CT-0126 and the CNRS Groupe de Recherche "GDR Exobiologie" (GDR 1877).

References

1 *The Molecular Origins of Life*, ed. A. Brack, Cambridge University Press, Cambridge, UK, 1998.
2 W. M. Irvine, P. Friberg, N. Kaifu, H. E. Mathews, Y. C. Minsh, M. Ohishi and S. Ishikawa, *Astron. Astrophys.*, 1990, **229**, L9–L12.
3 W. A. Schutte, A. G. G. M. Tielens, D. C. B. Whittet, A. Boogert, P. Ehrenfreund, Th. de Graauw, T. Prusti, E. F. van Dishoeck and P. Wesselius, *Astron. Astrophys.*, 1996, **315**, L333.
4 W. A. Schutte, A. C. A. Boogert, A. G. G. M. Tielens, D. C. B. Whittet, P. A. Gerakines, J. E. Char, P. Ehrenfreund, J. M.

Greenberg, E. F. van Dishoek, Th. de Graauw, *Astron. Astrophys.*, 1999, **343**, 966.
5 M. C. McCarthy and P. Thaddeus, *Chem. Soc. Rev.*, 2001, **30**, 177.
6 P. A. Burgers, A. A. Mommers and J. L. Holmes, *J. Am. Chem. Soc.*, 1983, **105**, 5976.
7 E. Uggerud, W. Koch and H. Schwartz, *Int. J. Mass Spectrom. Ion Processes*, 1986, **73**, 187.
8 E. Herbst, *Chem. Soc. Rev.*, 2001, **30**, 168.
9 H. Cottin, M. C. Gazeau and F. Raulin, *Planet. Space Sci.*, 1999, **47**, 1141.
10 P. Ehrenfreund, L. d'Hendecourt, S. B. Charnley and R. Ruiterkamp, *J. Geophys. Res.*, 2001, **106**, 33 291.
11 (*a*) M. Schwell, S. Leach, K. Hottmann, H. W. Jochims and H. Baumgärtel, *Chem. Phys.*, 2001, **272**, 77; (*b*) S. Leach, M. Schwell, D. Talbi, G. Berthier, K. Hottmann, H. W. Jochims and H. Baumgärtel, *Chem. Phys.*, 2002, in press.
12 M. Schwell, F. Dulieu, H. W. Jochims, J.-L. Lemaire, J.-H. Fillion, H. Baumgärtel and S. Leach, *J. Phys. Chem. A*, 2002, in press.
13 M. Suto, X. Wang and L. C. Lee, *J. Phys. Chem.*, 1988, **92**, 3764.
14 K. Tabayashi, J.-I. Aoyama, M. Matsui, T. Hino and K. Saito, *J. Chem. Phys.*, 1999, **110**, 9547.
15 C. R. Brundle, D. W. Turner, M. B. Robin and H. Basch, *Chem. Phys. Lett.*, 1969, **3**, 292.
16 R. K. Thomas, *Proc. R. Soc. London, Ser. A*, 1972, **A331**, 249.
17 I. Watanabe, Y. Yokoyama and S. Ikeda, *Chem. Phys. Lett.*, 1973, **19**, 406.
18 T. Ari and J. B. Hasted, *Chem. Phys. Lett.*, 1982, **85**, 153.
19 C. Fridh, *J. Chem. Soc., Faraday Trans. 2*, 1978, **74**, 190.
20 T. Ari and H. H. Güven, *J. Electron Spectrosc. Relat. Phenom.*, 2000, **106**, 29.
21 A. Hoxha, R. Locht, B. Leyh, D. Dehareng, K. Hottmann, H. W. Jochims and H. Baumgärtel, *Chem. Phys.*, 2000, **260**, 237.
22 S. Bell, T. L. Ng and A. D. Walsh, *J. Chem. Soc., Faraday Trans. 2*, 1975, **71**, 393.
23 W. C. Price and W. M. Evans, *Proc. R. Soc. London, Ser. A*, 1937, **162**, 110.
24 T. L. Ng and S. Bell, *J. Mol. Spectrosc.*, 1974, **50**, 166.
25 S. R. Langford, A. D. Batten, M. Kono and M. N. R. Ashfold, *J. Chem. Soc., Faraday Trans.*, 1997, **93**, 3757.
26 R. W. Davis, A. G. Robiette, M. C. L. Gerry, E. Bjarnov and G. Winnewisser, *J. Mol. Spectrosc.*, 1980, **81**, 93.
27 E. Bjarnov and W. H. Hocking, *Z. Naturforsch.*, 1978, **33A**, 610.
28 W. H. Hocking, *Z. Naturforsch.*, 1976, **31A**, 1113.
29 M. T. Nguyen, *Chem. Phys. Lett.*, 1989, **163**, 344.
30 K. Takeshita, *Chem. Phys.*, 1995, **195**, 117.
31 R. C. Millikan and K. S. Pitzer, *J. Chem. Phys.*, 1957, **27**, 1305.
32 J. E. Bertie and K. H. Michelian, *J. Chem. Phys.*, 1982, **76**, 886.
33 I. C. Hisatsune and J. Heicklen, *Can. J. Spectrosc.*, 1973, **8**, 135.
34 S. D. Peyerimhoff and R. J. Buenker, *J. Chem. Phys.*, 1969, **50**, 1846.
35 D. Demoulin, *Chem. Phys.*, 1976, **17**, 471.
36 S. Itawa and K. Morokuma, *Theor. Chim. Acta*, 1977, **44**, 323.
37 H. Basch, M. B. Robin and N. A. Kuebler, *J. Chem. Phys.*, 1968, **49**, 5007.
38 M. B. Robin, *Higher Excited states of Polyatomic Molecules*, vol. III, Academic Press, Inc., London, 1985, p. 310.
39 F. Ioannoni, D. C. Moule and D. J. Clouthier, *J. Phys. Chem.*, 1990, **94**, 2290.
40 E. E. Barnes and W. T. Simpson, *J. Chem. Phys.*, 1963, **39**, 670.
41 W. T. Simpson, *J. Am. Chem. Soc.*, 1962, **84**, 2853.
42 M. B. Robin and W. T. Simpson, *J. Chem. Phys.*, 1962, **36**, 580.
43 S. Nagakura, K. Kaya and H. Tsubomura, *J. Mol. Spectrosc.*, 1964, **13**, 1.
44 M. B. Robin, *Higher Excited states of Polyatomic Molecules*, vol. II, Academic Press, Inc., London, 1974, p. 144 and 154.
45 J. Schirmer, L. S. Cederbaum, W. Domke and W. von Niessen, *Chem. Phys. Lett.*, 1978, **57**, 582.
46 A. W. Potts, T. A. Williams and W. C. Price, *Faraday Discuss. Chem. Soc.*, 1972, **54**, 104.
47 K. Kimura, S. Katsumata, T. Yamazaki and H. Wakabayashi, *J. Electron Spectrosc. Relat. Phenom.*, 1975, **6**, 41.
48 T. Nishimura, G. G. Meisels and Y. Niwa, *J. Chem. Phys.*, 1989, **91**, 4009.
49 W. von Niessen, G. Bieri and L. Asbrink, *J. Electron Spectrosc. Relat. Phenom.*, 1980, **21**, 175.